OPTIMIZING THE PERFORMANCE OF P3HT-BASED PHOTODETECTOR BY TUNING THE COMPOSITION OF OXCBA

SYAZA NAFISAH HISAMUDDIN

FACULTY OF SCIENCE
UNIVERSITI MALAYA
KUALA LUMPUR

2021

OPTIMIZING THE PERFORMANCE OF P3HT-BASED PHOTODETECTOR BY TUNING THE COMPOSITION OF OXCBA

SYAZA NAFISAH HISAMUDDIN

DISSERTATION SUBMITTED IN FULFILMENT OF THE REQUIREMENTS FOR THE DEGREE OF MASTER OF SCIENCE

DEPARTMENT OF PHYSICS
FACULTY OF SCIENCE
UNIVERSITI MALAYA
KUALA LUMPUR

2021

UNIVERSITI MALAYA

ORIGINAL LITERARY WORK DECLARATION

Name of Candidate: **SYAZA NAFISAH BINTI HISAMUDDIN**

Matric No: **17141779/3**

Name of Degree: **MASTER OF SCIENCE**

Title of Project Paper/Research Report/Dissertation/Thesis ("this Work"): **OPTIMIZING THE PERFORMANCE OF P3HT-BASED PHOTODETECTOR BY TUNING THE COMPOSITION OF OXCBA**

Field of Study: **EXPERIMENTAL PHYSICS**

I do solemnly and sincerely declare that:

(1) I am the sole author/writer of this Work;
(2) This Work is original;
(3) Any use of any work in which copyright exists was done by way of fair dealing and for permitted purposes and any excerpt or extract from, or reference to or reproduction of any copyright work has been disclosed expressly and sufficiently and the title of the Work and its authorship have been acknowledged in this Work;
(4) I do not have any actual knowledge nor do I ought reasonably to know that the making of this work constitutes an infringement of any copyright work;
(5) I hereby assign all and every rights in the copyright to this Work to the University of Malaya ("UM"), who henceforth shall be owner of the copyright in this Work and that any reproduction or use in any form or by any means whatsoever is prohibited without the written consent of UM having been first had and obtained;
(6) I am fully aware that if in the course of making this Work I have infringed any copyright whether intentionally or otherwise, I may be subject to legal action or any other action as may be determined by UM.

Candidate's Signature Date:

Subscribed and solemnly declared before,

Witness's Signature Date:

Name:

Designation:

OPTIMIZING THE PERFORMANCE OF P3HT-BASED PHOTODETECTOR BY TUNING THE COMPOSITION OF OXCBA

ABSTRACT

Organic photodetectors (OPDs) have shown high responsivity and detectivity limits with fast response speed that are matched with commercially available inorganic photodetectors. The feasibility to tune the spectral response of the organic material and flexibility to use on curve substrate also give the advantage of using organic materials in the fabrication of OPDs. Nevertheless, there are still many challenges that need to be addressed to achieve a greater performance of an OPD device. In this work, the performance of organic-based photodetectors using poly(3-hexylthiophene) (P3HT) and *o*-xylenyl-C_{60}-bisadduct (OXCBA) as the donor and acceptor material, respectively, is reported aiming to improve the performance of P3HT-based OPD device. Four different ratios of 1:0.25, 1:0.50, 1:1.00 and 1:1.50 of P3HT:OXCBA binary blended thin films are prepared using spin-coating technique and used as photoactive layers. The elemental composition and electronic properties of the materials are characterized using X-ray Photon Spectroscopy (XPS) and Ultraviolet Photon Spectroscopy (UPS). The optical properties of the thin films are characterized using Ultraviolet-visible (UV-vis) spectroscopy and the electrical performance for all ratios are characterized using current-voltage (I-V) measurement. Further, two blend ratios that show the best and the worst performance are characterized using Photoluminescence (PL) Spectroscopy, Atomic Force Microscopy, Raman Spectroscopy. It was found that the combination of P3HT and OXCBA demonstrates a wide spectral range of light absorption which covers the valley that has low light absorption, with the ratio of 1:0.50 demonstrates the best performance. The OPD devices with ratio 1:0.25 to 1:1.50 shows high photocurrent density (J_{ph}) from 8.09 mA/cm^2 to 25.27 mA/cm^2. Optimizing the ratio of photoactive layers dramatically

enhances the performance of OPDs, with the rise and decay time of 445 and 309 ms, respectively, recorded from 1:0.50 ratio. The optimized device has achieved high responsivity of 252.69 mA/W and specific detectivity of 1.85×10^{10} Jones at -1 V, and has shown good stability for over 336 hours. Aside from that, external quantum efficiency (EQE) of 52.77% and low surface roughness of 0.596 nm are obtained from the 1:0.50 P3HT: OXCBA device. These results imply a high potential of P3HT:OXCBA blend in the application of a photodetector.

Keywords: Organic photodetector; binary; OXCBA; P3HT

MENGOPTIMUMKAN PRESTASI PENGESAN CAHAYA BERASASKAN P3HT DENGAN MENGUBAH KOMPOSISI OXCBA

ABSTRAK

Peranti pengesan cahaya organik (OPD) telah menunjukkan nilai responsiviti dan pengesanan yang tinggi dengan kadar tindak balas pantas yang sepadan dengan aplikasi pengesan cahaya yang sedia ada di pasaran. Keupayaan untuk mengubah spektrum tindak balas dan juga fleksibiliti untuk digunakan pada substrat lengkung memberi kelebihan untuk menggunakan bahan organik di dalam pembuatan peranti OPD. Namun begitu, masih ada banyak cabaran yang perlu ditangani bagi mencapai tahap prestasi peranti OPD yang lebih tinggi. Kajian ini melaporkan prestasi OPD menggunakan poly (3-hexylthiophene) (P3HT) dan juga *o*-xylenyl-C_{60}-bisadduct (OXCBA) sebagai bahan penderma dan penerima dengan tujuan untuk mempertingkatkan prestasi peranti OPD yang berasaskan P3HT. Lapisan nipis daripada campuran P3HT: OXCBA dengan empat nisbah berbeza iaitu 1:0.25, 1:0.50, 1:1.00 dan 1:1.50 telah disediakan menggunakan teknik lapisan putaran dan digunakan sebagai lapisan fotoaktif. Komposisi unsur dan sifat electronik bagi bahan telah dicirikan menggunakan XPS dan UPS. Sifat-sifat optik bagi lapisan nipis dicirikan menggunakan spektroskopi UV-Vis dan prestasi elektrik untuk semua nisbah dicirikan menggunakan pengukuran I-V. Selanjutnya, dua nisbah yang menunjukkan prestasi terbaik dan terburuk dipilih dan dicirikan menggunakan spektroskopi PL, AFM dan RAMAN. Hasil kajian ini mendapati bahawa gabungan P3HT dan OXCBA menunjukkan spektrum penyerapan cahaya yang luas yang turut meliputi kawasan lembah yang mempunyai nilai serapan cahaya yang rendah, dan nisbah 1:0.50 telah menunjukkan prestasi yang terbaik. Peranti-peranti OPD dengan nisbah 1:0.25 sehingga 1:1.50 telah menunjukkan nilai ketumpatan arus litar pintas (J_{ph}) yang tinggi dari 8.09 mA/cm^2 hingga 25.27 mA/cm^2. Mengoptimumkan nisbah lapisan fotoaktif secara dramatiknya dapat meningkatkan prestasi peranti OPD, dengan masa kenaikan dan

penurunan sebanyak 445 dan 309 dicatatkan dari nisbah 1:0.50. Peranti dengan nisbah optimum telah mencapai nilai responsiviti yang tinggi sebanyak 252.69 mA/W dan pengesanan spesifik sebanyak $1.85x10^{10}$ Jones pada -1 V, dan peranti itu telah menunjukkan tahap stabiliti yang baik selama lebih dari 336 jam. Selain itu, nilai kecekapan kuantum luaran (EQE) sebanyak 52.77% dan kekasaran permukaan yang rendah sebanyak 0.596 nm juga telah diperoleh dari peranti P3HT:OXCBA dengan nisbah 1:0.50. Hasil ujian-ujian ini menunjukkan bahawa gabungan P3HT:OXCBA mempunyai potensi yang tinggi di dalam aplikasi peranti pengesan cahaya.

Kata kunci: Peranti pengesan cahaya organik; binari; OXCBA; P3HT

ACKNOWLEDGEMENTS

First and foremost, my deepest thanks go to my supervisor, Dr Azzuliani Supangat for her generosity in dedication and continuous support throughout this project. Without her guidance, I might have tumbled down in the middle of the period. She taught me to think critically, broaden my knowledge and learn how to write. I have been amazingly fortunate to work under her who gave me the freedom to explore my research and thoughtful discussion during this work. I also want to thank my coordinator, Dr Shahino Mah for answering my countless questions, explaining the experimental setup and encouraging me in difficult times. I have learnt a lot from their endless patience in all the discussions and I appreciate them for tirelessly correcting my paper as well as this manuscript.

Most importantly, I am also deeply indebted to my family, especially both of my parents, Hisamuddin Bin Kamarollzaman and Maziana Binti Murad for their endless support and unconditional love. They always have faith in me and continuously encourage, support and help me to pursue my studies. Without their proper care and education, I would never manage and qualify enough to complete my master's degree.

I also especially express my gratitude to my lab partners, Siti Anis Khairani and Afiq Anuar for helping me throughout the period. Both of them are very good friends and supporters during my master journey. They always cared about my research and health during the semester when I was busy doing both teaching and research work. Last but not least, a special mention goes to my friends in LDMRC for supporting me from behind and have helped me whenever I need it. All the people I mentioned above and their contributions will not be forgotten.

TABLE OF CONTENTS

LIST OF FIGURES

LIST OF TABLES

LIST OF SYMBOLS AND ABBREVIATIONS

J_d	:	Dark current density
eV	:	Electron volt
V_{oc}	:	Open-circuit voltage
E_g	:	Optical band gap
J_{ph}	:	Photocurrent density
hv	:	Photon energy
π	:	Pi bond
J_{sc}	:	Short-circuit current density
D^*	:	Specific Detectivity
λ	:	Wavelength
ϕ	:	Work function
AFM	:	Atomic Force Microscopy
Al	:	Aluminium
Au	:	Gold
BE	:	Binding energy
BHJ	:	Bulk heterojunction
C_{60}	:	Fullerene
CV	:	Cyclic-voltammetry
DI	:	Deionized water
EQE	:	External Quantum Efficiency
HOMO	:	Highest Occupied Molecular Orbital
HTL	:	Hole Transport Layer
IPA	:	Isopropanol
ITO	:	Indium Tin Oxide

I-V	:	Current-voltage
KE	:	Kinetic energy
LiF	:	Lithium Fluoride
LUMO	:	Lowest Unoccupied Molecular Orbital
MoO_3	:	Molybdenum Oxide
N_2	:	Nitrogen
OPD	:	Organic photodetector
OXCBA	:	*o*-xylenyl-C_{60}-bisadduct
OXCMA	:	*o*-xylenyl-C_{60}-monoadduct
OXCTA	:	*o*-xylenyl-C_{60}-trisadduct
P3HT	:	Poly (3-hexylthiphene)
$PC_{61}BM$	:	Phenyl-C_{61}-butyric acid methyl ester
PEDOT:PSS	:	Poly (3,4 –ethylenedioxy-thiophene) –Poly (styrene sulfonate)
PL	:	Photoluminescence
PVD	:	Physical Vapour Deposition
R	:	Responsivity
RMS	:	Root mean square
UHV	:	Ultra-high vacuum
UPS	:	Ultraviolet Photoelectron Spectroscopy
UV	:	Ultraviolet
UV-Vis	:	Ultraviolet-visible
XPS	:	X-ray Photoelectron Spectroscopy
ZnO	:	Zinc Oxide

CHAPTER 1: INTRODUCTION

1.1 Introduction

Photodetectors are one of the key components in many optoelectronic devices that facilitate the conversion of light into electrical signals. It primarily works based on light absorption of a material that then generates photocurrent within the device which further be processed by readout electronics. Alexandre Edmond Becquerel first reported the discovery on photocurrent generation when being exposed to light in 1836 but the explanation on this phenomenon was only given by Vladimir Zworykin in 1936 (Zworykin, Morton, & Malter, 1936) that identified three kinds of light detection: by potential barrier crossing, linked state-free transition and via electron-hole pair (the mechanism that governs photodetection in photodetectors). Since then, numerous studies on photoconductivity phenomena have been conducted which suggest solid material such as selenium can generate current without being subjected to heat or any mechanical movement (Adams & Day, 1877).

Studies in the early 19th century remark the beginning of organic electronics when Pochettino and Volmer reported the photoconductivity of organic material, anthracene when exposed to electromagnetic radiation in 1906 and 1913, respectively (Moliton & Hiorns, 2012). Later, Kallmann and Pope had fabricated the first solar cell device and observed the photovoltaic effect in a single crystal of anthracene that results in low efficiency around 0.1% (Kallmann & Pope, 1959). Further, in 1977, Hideki Shirakawa and Edwin J. Louis also discover polyacetylene, a conducting polymer with metallic electrical transport by halogen doping which indicates photovoltaic effect take parts at metal and polymer interfaces (Shirakawa, Louis, MacDiarmid, Chiang, & Heeger, 1977; Shirakawa, McDiarmid, & Heeger, 2003). This stimulates the discoveries of a whole new branch of materials known as organic semiconductors and groundbreaking invention of organic electronics such as organic light emitting diode, and organic photovoltaic.

Later, in 1986, Tang et al. reported the breakthrough in thin film bilayer heterojunction in organic small molecule photovoltaic cells and achieved energy conversion efficiency of 1% (Tang, 1986). In 1992, Sariciftci and Morita discovered that phase separation in donor and acceptor is crucial to achieve proper carrier transport channel between a conjugated polymer and fullerene derivatives (Sariciftci, Smilowitz, Heeger, & Wudl, 1992). In the next year of that, Sariciftci also demonstrated the first planar heterojunction in polymer photodiodes and solar cells. The research on organic semiconductor devices evolved rapidly until 1995 when Yu et al. set a landmark in bulk heterojunction (BHJ) solar cell and photodiode with polymer-polymer and polymer–fullerene blends (Yu & Heeger, 1995).

Today, organic photodetectors (OPDs) have become a focus of innovative research and reach a mature technology level application such as in imaging, fibre optic communication, remote sensing and telecommunication. Light, with a large spectral wavelength ranging from Ultraviolet (UV) to Infrared (IR), carries valuable information which needs to be detected fast and efficiently for further digital processing. Photodetectors are built with a diverse range of semiconductor materials to sense different range of light spectrum. For example, photodetectors that work in the visible range are used in indirect conversion x-ray imaging, biometric fingerprint scanner as well as in surface gesture recognition. Apart from that, visible light OPDs are also utilized for presence sensors and also in digital cameras. Flexibility, thin and lightweight nature of wearable organic electronics are considered to be a remarkable property for the new generation of low power optoelectronic devices.

1.2 Motivations

At present, most commercially available photodetectors are still dominated by inorganic semiconductors that are made of non-carbon-based material such as silicon,

gallium nitride or gallium arsenide due to their excellent charge carrier mobility. Despite having good stability and high performance, the fabrication of these devices usually includes complex processes as it needs to be done in a vacuum condition and requires high manufacturing cost. Their rigid structure also restricts the shape of the photodetector, making them to be inflexible for various applications (Zhao, Xu, Niu, Zhang, & Zhang, 2020).

Unlike inorganic semiconductor, organic electronics provides huge potential for mass production with an inexpensive cost (A. Singh, Dey, & Iyer, 2017). Organic semiconductors are processed in an ambient condition and are therefore compatible with flexible substrates. Moreover, they provide a wide range of tailor-made materials which are tunable to work at selective electromagnetic spectrum. The bandgap of an organic material can also be tuned by chemical substitution without changing the electronic properties of the material. Further, it offers several more advantages including lightweight, mechanical flexibility, and environmentally friendly (Ji, Lee, & Oh, 2019; Salamandra et al., 2020; Yang & Ma, 2019).

Nevertheless, stability issues still become a bottleneck in the commercialization of organic devices. The nature of transport properties limits their efficiency as the charge carrier mobility in an organic semiconductor is much lower compared to the inorganic semiconductor. The performance of the device is also highly dependent on the thickness and morphology of the photoactive layer and contact between every layer. Apart from that, organic semiconductor is highly sensitive to environmental influence such as scratches or degradation. Therefore, continuous study has been conducted to achieve devices that not only perform greatly but also stable for a long period of time.

To date, P3HT and PCBM devices can be regarded as model systems to tackle the issues that arise in an OPD device. To improve the performance of the OPD device,

OXCBA has been designed as an effort to develop a novel material that could replace PCBM but the literature about this combination is still limited to the solar cell application. The high LUMO level of OXCBA is proven to increase the open-circuit voltage (V_{oc}), thus improve the device performance. As a good solar cell can also be a good photodetector, this study is carried out to analyze the photo-sensing performance in P3HT and OXCBA OPD device.

1.3 Objectives

The aim of this study is to introduce *o*-xylenyl-C_{60}-bisadduct (OXCBA) as a novel n-type organic material in solution-processed Poly (3-hexylthiophene) (P3HT) OPD device by tuning the composition of OXCBA in the device, thereby targeting to achieve high responsivity and detectivity of the device and improve the overall performance of the device. Initially, characterization on P3HT:OXCBA thin film is conducted and analyzed in terms of their optical, structural, and morphological properties. Next, the P3HT:OXCBA blended solution is introduced into the device and their electrical and photodetection properties are analyzed.

The host electron donor, P3HT is a conjugated polymer and is well known to have high regioregularity due to π-π stacking of its rigid backbone and side chains. On the other hand, OXCBA is categorized as a small molecule because its molecular weight is much lower compared to the conducting polymer. This class of material tends to crystallize especially when a solution-process technique is used. Through the incorporation and optimization of OXCBA in P3HT-based devices, the objectives of achieving an enhanced solution-processed OPD is also being realized.

Hence, this thesis studies can be summarized aiming to achieve the following objectives:

- To achieve a broad spectral range of optical absorption in the whole visible region.

- To fabricate a highly responsive P3HT:OXCBA OPD device that can achieve over 100 mA/W.
- To obtain fast response OPD that are stable for a long period of time.

To the best of my knowledge, investigation on the properties of OXCBA and incorporation of OXCBA in photodetection devices is not yet available from literature, making it a novelty in this study. In this study, we also provide a new investigation on the effect of different concentrations of OXCBA in P3HT-based OPD, thus determining the compatibility of OXCBA with P3HT by evaluating their photo-sensing performance. The combination of the materials is expected to improve the optical absorption range, generate more charge carriers and improve the OPD performance. Besides, this study also provides the elemental study of OXCBA using X-ray Photon Spectroscopy (XPS) and Ultraviolet Photon Spectroscopy (UPS) analysis as the previous study only determine the energy levels using CV analysis, thereby giving more accurate data.

1.4 Thesis outline

This thesis covers 5 chapters that discuss the effect of OXCBA in P3HT-based OPD. Chapter 1 outlines the importance of organic devices as well as the motivation and objectives of this work.

Chapter 2 presents the basic principle and operating mechanism of a photodetector that includes light absorption, exciton generation, charge transfer and charge collection at the electrode. Further, literature on materials used in this work, P3HT and OXCBA is elaborated in this chapter as well as previous studies that are related to this research.

Next, Chapter 3 discusses the fabrication process of the device as well as the characterization technique used in this work. The background research on each instrument is briefly explained.

Chapter 4 presents the experimental results obtained from the characterization. The first part discusses the results of thin film characterization and the second part will discuss the performance of the device.

Finally, Chapter 5 presents the conclusion that summarizes the overall work done in this research as well as suggestions on possible work to improve the performance of OPD devices in the future.

CHAPTER 2: LITERATURE REVIEW

2.1 Introduction

This chapter discussed the physics behind organic photodiode and organic materials used in-depth. The first part of this chapter explains the device structure and basic principle of an OPD. Next, the operation principle of OPD devices which include the charge injection, transport and collection are explained followed by a discussion on the importance of the energy level alignment of material. This chapter presents literature reviews on P3HT and OXCBA. This chapter ends with elaboration on significant works that utilize both materials in organic devices.

2.2 Organic Photodetector (OPD)

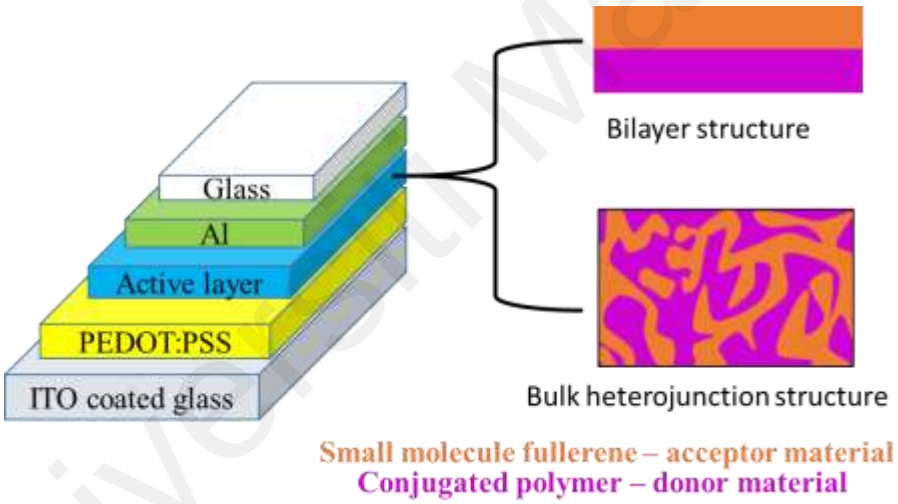

Figure 2.1: Basic structure of an OPD device.

An OPD is an optical sensor that converts the light signal into electricity. The standard photodetector structure is basically the same as a solar cell. It consists of an anode, photoactive layer and cathode. The photoactive layer usually exists in multilayer and BHJ structure (Figure 2.1). In a multilayer structure, the donor and acceptor material are deposited separately to form a similar junction as a p-n junction diode. This structure gives the advantage of having a controlled blend morphology with defined thickness around 100 to 200 nm for each layer. On the other hand, the BHJ structure is formed by

blending the materials together before being deposited onto a substrate (T. H. Lee et al., 2020).

Thick active layer in a multilayer structure device could absorb more light and generate more photocurrent, but it could also become a limitation as the diffusion length of exciton is only around 10 nm, which is much shorter than the film thickness (Benten, Mori, Ohkita, & Ito, 2016). Therefore, the active layers of an OPD are often based on a BHJ structure that consists of intermixed percolating pathways of donor and acceptor phases. Aside from that, the BHJ structure provides a larger interface area of the photoactive layer that helps to facilitate exciton diffusion and the bi-continuous network enables efficient charge transport to the relevant electrodes (Y. Li et al., 2020).

A photodetector also operates in almost the same concept as a solar cell but with several differences. Solar cells rely on optical power to generate current and voltage without any external power supply, whereas photodetectors operate by applying a reverse bias to provide faster charge dissociation, transport and collection when light is illuminated on the device. Electric fields will build up in the presence of external bias due to the difference in the work function of the material. The difference in the internal electric field between photoactive layers helps to separate the exciton into free carriers. Apart from that, the negative bias helps to improve the photocurrent generated, photosensitivity and response speed of a photodetector (Kielar, Dhez, Pecastaings, Curutchet, & Hirsch, 2016). It also reduces interface polarization. However excessive reverse-biased voltage supplied may result in higher noise and may cause breakdown and degradation of the device.

2.3 Operation Principles in OPD

The operation principle of a photodetector involves four stages which include light absorption, charge carrier generation, carrier transport and collection at the electrode.

Usually, an efficient OPD consists of at least two or more materials, with different HOMO (Highest Occupied Molecular Orbital) and LUMO (Lowest Unoccupied Molecular Orbital) level. The HOMO levels are responsible for hole transport while LUMO levels are responsible for electron transport (Dechun, 2013; S. P. Singh, Sellinger, & Dodabalapur, 2010).

Figure 2.2 below shows a schematic process of the charge carrier hopping mechanism in an OPD device. When light is illuminated onto the sample, electrons in an organic semiconductor will be excited from HOMO to LUMO level, thus forming an exciton. Exciton is an electron-hole pair that is bounded by a coulombic attraction force. This is similar to the excitation of electrons from the valence band to the conduction band in inorganic semiconductors (W. Li & Kwok, 2012). Once exciton is formed, they can diffuse towards the donor-acceptor interface and dissociate there. The potential difference of material should be larger than exciton binding energy to facilitate carrier transport and avoid recombination. Next, the free carriers will either be transported to their respective electrode or recombine geminately with opposite charges. This movement of electrons and holes are in hopping mode. Electrons should move from the LUMO of donor towards the cathode, whereas holes should move from the HOMO of donor, reaching anode. This whole process will lead to photocurrent generation.

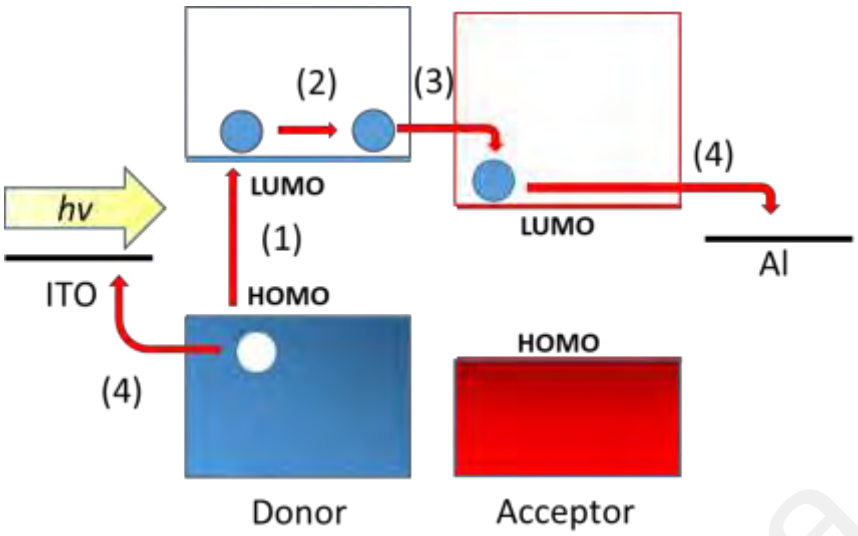

Figure 2.2: Schematic description of the electronic transition in donor and acceptor blend; (1) light absorption, (2) exciton diffusion, (3) charge transfer and (4) charge collection at the electrodes.

The selection of material is important in the fabrication of an efficient OPD to ensure proper alignment on the energy level. The work function of anode needs to be high to align with the HOMO of the active layer to allow efficient hole injection. On the other hand, the work function of cathode is required to be low to inject electrons from the LUMO of the active layer. As for the material, the HOMO and LUMO level of donor material should be lower than that of an acceptor. Otherwise, hole can transfer itself to the acceptor. This will affect the carrier mobility, increase carrier recombination along with energy loss.

2.4 Organic semiconductor

An organic semiconductor is basically a π-bonded molecular solid that is made up of carbon and hydrogen atoms that are alternating in single and double bonds. They can largely be classified into two categories, which is the polymer and small molecule, based on their molecular weight. Polymer is a complex molecule with a very high molecular weight (> 20,000 g/mole) while a small molecule has a very low molecular weight (<1000 g/mole) (Ballantyne et al., 2008; Dechun, 2013). Generally, there are two types of charge

carrier present in an organic material, which is electron and hole. Electrons are physical particles that are negatively charged, whereas holes are theoretical concepts that represent void of electrons and are positively charged. An organic semiconductor can be classified as an electron donor or electron accepting material according to the majority carrier species in the material. In this study, P3HT and OXCBA are selected based on their optoelectronic properties. P3HT will act as electron donor material while OXCBA act as electron accepting material. The molecular structures for P3HT and OXCBA are shown in Figure 2.3 below.

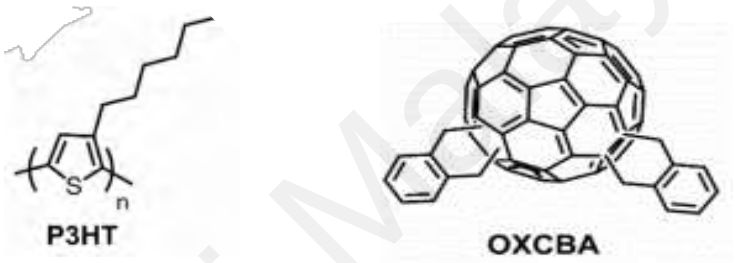

(a) (b)

Figure 2.3: Molecular structure of (a) P3HT and (b) OXCBA. (D. J. Kang et al., 2013; H. J. Kim et al., 2014)

2.4.1 Poly (3-hexylthiophene) (P3HT)

P3HT is well known as π-conjugated polymer and has been widely used as a promising electron-donating material owing to its relatively high hole mobility, solution-processability properties, and good stability (Holliday et al., 2016). Structurally, the polythiophene rigid backbone and the arrangement of its alkyl side chain allows efficient π-π stacking of the conjugated polymer, thus providing high regioregularity of the material (Xiao, Tang, Yang, Wei, & Zhou, 2017). Many literatures have reported the connection between regioregularity and crystallinity of the material. While good crystallinity could enhance the performance of photodetectors, excessive crystallinity

could also lead to device failure. For this reason, the blending of P3HT with fullerenes is favorable to obtain their optimum surface morphology.

Aside from that, P3HT has a high-lying HOMO level (~5.0 eV) that could guarantee efficient carrier transfer. Despite that, P3HT single layer devices would face a problem as the electric field from the electrodes would be insufficient to split the exciton and resulting in the recombination of holes and electrons without reaching the electrodes. Therefore, P3HT is usually blended with fullerene derivatives such as phenyl-C_{61}-butyric acid methyl ester ($PC_{61}BM$) and its corresponding C_{71} derivatives, $PC_{71}BM$ to provide the necessary energy offset for exciton dissociation.

2.4.2 *O*-xylenyl-C_{60}-bisadduct (OXCBA)

Besides conjugated polymer, fullerene and their derivatives are widely deployed because of their high electron mobility, good charge transfer properties at the interface of photoactive material and ability to form favourable nanoscale networks with the donor polymer. In a recent study, another fullerene derivative, OXCBA has gained attention as it provides comparable performance to PCBM (H. Kim, Park, Park, & Hwang, 2016; K.-H. Kim et al., 2011).

In the molecular structure of OXCBA, *o*-xylenyl solubilizing groups are effectively tethered to fullerene with an exact ratio of 2:1. This alteration disrupts the π-conjugated system of fullerene and reduces the orbital number of parent fullerene from 60 sp^2 to 56 sp^2 carbon atoms (K.-H. Kim et al., 2011). As a result, there is a decrease in the crystallinity of the fullerene derivatives and also a reduction in its electron affinity.

In addition to that, the compact CH_2 group that is tethered to fullerene increases the LUMO level of OXCBA to be higher than PCBM. According to Tajbakhsh, high levels

of LUMO of the acceptor can increase the value of open-circuit voltage (V_{oc}) in solar cell devices (Tajbakhsh, Kariminasab, Ganji, & Alinezhad, 2017).

As P3HT has a higher molecular weight than OXCBA, blending the two materials may result in a more compact molecular arrangement that will increase the interface density of the photoactive layer and provide a higher interpenetrating path for carrier transport. Moreover, the combination of P3HT and OXCBA is expected to cover a broad range of light absorption spectrum. P3HT as an individual component has an intense but narrow absorption band in visible range while OXCBA absorption coverage will provide complementary absorption at a lower wavelength. The composite blend is expected to broaden the absorption spectrum range so that more light will be absorbed and more photo-current can be generated. Although thicker layers may absorb more light, the blend ratio of the material needs to be optimized to avoid molecular disarrangement by excessive segregation between the material and maximize charge extraction.

2.5 Previous studies on P3HT and OXCBA-based devices

Since the last few decades, many studies have been conducted on organic semiconducting materials to replace the inorganic counterparts. Amongst them, P3HT has been widely used on account of its high carrier mobility, stable performance and good solubility in nontoxic solvents. P3HT has shown significant performance with performance over 5% and is suitable for photo-sensing application (Kadem, Hassan, & Cranton, 2016; X. Xu, Zhang, Yu, Li, & Peng, 2019). For instance, Treat et al. has used the combination of P3HT and PCBM to study the interdiffusion properties of P3HT and PCBM in bilayer structure devices. From this study, he found that PCBM small molecules are mobile and could diffuse in the ordered P3HT without disrupting the P3HT domain. Under heat treatment, PCBM aggregates and disperses in the disordered P3HT, thereby increasing the thickness of P3HT crystallite (Treat et al., 2011).

Apart from that, Shafian et al. also investigated the performance of P3HT:PCBM device in bilayer and BHJ structure. The concentration of P3HT used in this study is varied from 20 mg/ml to 60 mg/ml while the concentration of PCBM is fixed at 14 mg/ml, with the thickness of the photoactive layer ranging from 149 nm to 580 nm. This study managed to obtain a low dark current which is favourable as it indicates low noise, but the photocurrent density (J_{ph}) obtained is low due to the thick active layer (Shafian, Jang, & Kim, 2015). It is reported that the optimum thickness for the photoactive layer of an OPD is about 100 nm to 200 nm. P3HT has a higher molecular weight than PCBM, therefore increasing the concentration of P3HT will increase the thickness of the active layer. While thick active layers could enhance light absorption and increase exciton generation, it is also expected to reduce the device performance due to the unbalanced carrier transport and increase in recombination loss (Zhang et al., 2017). Many literatures have reported the use of weight ratios from 1:0.6 up to 1:1 in P3HT-based device, with a small excess of P3HT (Azimy, Hosseini, & Ramezanian, 2016; Dang, Hirsch, & Wantz, 2011; H. Kim, Park, Grimsdale, & Hwang, 2015; K.-H. Kim et al., 2012).

In 2019, Han et al. has introduced $PC_{71}BM$ into P3HT and 2,2′-((2Z,2′Z)-(((4,4,9,9-tetrakis(4-hexylphenyl)-4,9-dihydro-sindaceno[1,2-b:5,6-b′]dithiophene- 2,7-diyl)bis(4-((2-ethylhexyl)oxy)thiophene-5,2- diyl))bis-(methanylylidene))bis(5,6-difluoro-3-oxo-2,3-dihydro-1H-indene-2,1- diylidene))dimalononitrile (IEICO-4F) device. The addition of $PC_{71}BM$ into the P3HT:IEICO-4F device increases the light absorption bandwidth and improves the surface morphology of the active layer. The cascade energy alignment of the material (ITO/ZnO/P3HT:IEICO-4F:$PC_{71}BM$:MoO_3:Ag) also helps to enhance the charge mobility, leading to efficient charge transfer (Han, Zhang, Zhang, Zhao, & Yu, 2019).

While many conjugated polymers have been designed, the choices for small molecule fullerenes are still limited. In 2011, Kim et al. have first developed OXCBA along with other *o*-xylenyl multiadduct derivatives; mono-, and tris-adducts (OXCMA, OXCTA). The 3 types of small molecules can be differentiated by different numbers of solubilizing groups that are tethered to fullerene. Among them, OXCBA shows great compatibility with P3HT with the highest efficiency compared to P3HT:PCBM control device and other multiadducts fullerene devices. He also found that P3HT:OXCBA device has great stability that is up to 18 months at room temperature without illumination.

In the following year, Kim et al. have introduced various substituents on the xylenyl group of OXCBA to examine the effect of structural changes in OXCBA on their photovoltaic performances. It is reported that changes in the molecular structure of OXCBA could tune the hydrophobicity of OXCBA derivatives and affect the miscibility and interfacial interaction with P3HT. OXCBA normal type devices were also found to exhibit 5% improvement compared to inverted type devices. However, their efficiency reduced to around 50% of its initial value within a week (K.-H. Kim et al., 2012).

Afterwards, another study was conducted by Kang et al, in 2013, to study the effect of OXCBA and OXCTA as a ternary acceptor in P3HT:OXCMA device. While many studies reported that ternary structure has better performance than binary structure, this study has proven otherwise. The study demonstrated that the binary structure composed of P3HT:OXCBA shows the best performance compared to ternary devices. In P3HT:OXCMA device, the addition of OXCTA could either produce synergistic energy offset by bridging P3HT and OXCMA molecules or become a carrier trapping site. The result highlights the importance of synergistic energy offset of the material. The unmatched HOMO and LUMO level would restrict the carrier mobility, give rise to the

unbalanced carrier transport and carrier recombination, thereby reducing the efficiency. (H. Kang et al., 2013).

Later in 2015, another study has reported the properties of methyl and dimethyl group of OXCBA and its multiadduct derivatives. In this study, the presence of methyl group substituents is reported to improve the solubility of multiadduct fullerene, therefore increasing the molar absorption coefficient of the material. However, it is observed that the absorption of modified OXCTA and the performance of devices containing fullerene trisadduct decrease which probably results from the increased disorder of the fullerene caused by the bulky trisadduct molecule (H. Kim et al., 2015). A similar result is observed in P3HT and trimethylsilyl *o*-xylenyl-substituted bis-adduct fullerene derivative (TMS-OXCBA) device conducted in 2016 (H. Kim et al., 2016). In this study, the TMS-OXCBA device exhibit unbalance amount of electron and hole, leading to reduced performance of the device. In essence, the addition of TMS as solubilizing group along with the presence of multiadduct isomer would increase the disorder of P3HT. It would prevent efficient packing of fullerene and decrease electron transport through fullerene.

Table 2.1: Strength and weakness observed from literature that provides in-depth analysis on P3HT and OXCBA devices.

References	Strength	Weakness
(Treat et al., 2011)	Miscibility of PCBM could affect the growth of P3HT crystallites.	The bilayer structure results in a thick photoactive layer (~200 nm).
(Shafian et al., 2015)	Low dark current density (J_d) obtained.	Low photocurrent density (J_{ph}) due to the thick active layer.
(Han et al., 2019)	Achieved broad spectral range with high detectivity limit (around 10^{12} Jones).	Complex fabrication of the device due to the presence of ZnO and MoO_3 as interlayer.
(K.-H. Kim et al., 2011)	OXCBA showed the highest efficiency compared to other multiadduct derivatives.	The presence of lithium fluoride (LiF) complicates the fabrication of the device.
(K.-H. Kim et al., 2012)	Normal type P3HT:OXCBA device shows improvement around 5 % compared to inverted type device.	Performance of normal type devices deteriorates to about 50% of its initial value within a week.
(H. Kang et al., 2013)	Binary structure devices show better performance compared to the ternary structure.	The presence of LiF complicates the fabrication process.
(H. Kim et al., 2015)	Methyl and dimethyl groups increase the molar absorption coefficient of the multiadduct derivatives.	An overly smooth surface may cause homogeneous separation between polymer and fullerene derivatives and cause imbalance carrier transport.
(H. Kim et al., 2016)	P3HT:PCBM device shows better performance compared to P3HT:TMS-OXCBA device.	Less balanced charge carrier in P3HT:TMS_OXCBA device.

CHAPTER 3: METHODOLOGY

3.1 Introduction

In this chapter, the process of fabricating an OPD device and the principle behind each measuring equipment used are presented. The first part of this chapter describes the preparation of substrate which includes substrate cleaning and plasma etching treatment. This chapter also explains the preparation of organic solvent and fabrication process for thin film and OPD devices using solution processing spin-coating technique and vacuum deposition system. The subsequent section describes the measurements carried out for thin film that include the determination for the film thickness. This section also presents the principles behind ultraviolet-visible (UV-Vis) spectroscopy, photoluminescence (PL) spectroscopy, Raman spectroscopy, atomic force microscopy (AFM), X-ray photoelectron spectroscopy (XPS) and ultraviolet photoelectron spectroscopy (UPS). Lastly, the electrical characterization of the OPD devices such as current-voltage (I-V) and external quantum efficiency (EQE) characterization technique are explained.

3.2 Substrate preparation

Glass and quartz were used for the characterization of thin film while pre-patterned ITO substrate was used for the fabrication of an OPD device. The ITO substrate is commonly used as an anode due to its transparency which could allow light to pass through. It also has a higher work function that allows holes to be easily injected to the HOMO of organic material. To ease the fabrication of an OPD device, a pre-patterned ITO glass substrate was used in this work. They were purchased from Ossila, United Kingdom with dimensions of 15 mm x 20 mm x 1.1 mm (L x W x H). As seen in Figure 3.1, the patterned ITO-coated glass consists of six different pixels with an active area of 0.045 cm^2 (1.5 mm x 3 mm) and each of the pixels is attributable to one device.

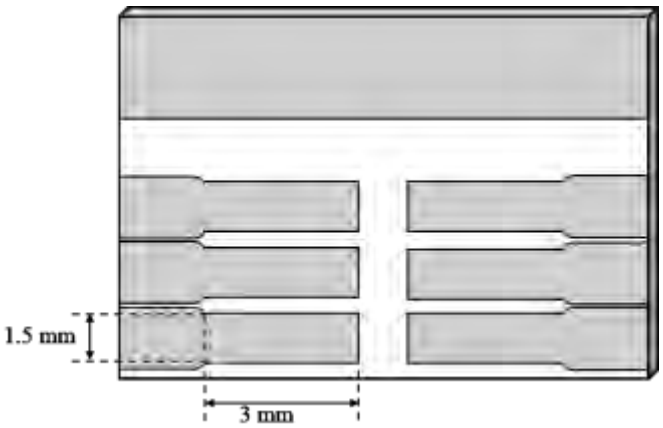

Figure 3.1: The dimensional drawing of patterned ITO-coated glass substrate used in this work. The grey areas refer to the surface that has ITO coating and the white area refer to glass.

Prior to the fabrication, the patterned ITO-coated glass substrates were subsequently cleaned in an ultrasonic bath using soap water, deionized (DI) water, acetone and isopropyl alcohol (IPA) sequentially for 20 minutes each. This process is carried out to avoid any contamination on the surface of the substrate during the film deposition. Next, the substrate was dried with a nitrogen stream and treated with a surface etching process using oxygen plasma at 35 W for 5 minutes. The oxygen plasma treatment helps to remove contaminants and increase the work function of ITO (Maeng, Kim, Hong, & Park, 2016). More importantly, it improves the surface wettability using highly reactive oxygen radicals. In this process, the substrate was placed in an airtight chamber and the pressure inside the chamber is pumped down using vacuum to remove all air. To begin the treatment, oxygen will be directed into a low-pressure chamber where the potential difference between the two parallel plates causes the gas to be ionized and produce plasma. The excited plasma will collide with the substrate surface and change the surface geometry. The surface will undergo oxidation and the plasma ions will form hydroxyl groups on the surface. This treatment was done to make the ITO-glass surface hydrophilic and ensure good adhesion between the spin-coated layer and the substrate.

3.3 Organic material and solution

The materials, P3HT was purchased from Sigma Aldrich while OXCBA was obtained from Lumtec and used as received. The organic solutions were prepared by dissolving the organic materials in chloroform. Chloroform is the most favourable solvent in preparing the BHJ active layer structure due to the good solubility of P3HT and OXCBA in order to obtain crystal packing structure. In this work, P3HT was dissolved at an optimal fixed concentration of 15 mg/ml while the concentration ratio of OXCBA was tuned between 0.25 to 1.50 with respect to the concentration of P3HT in the same solvent. The combinations of P3HT and OXCBA were stirred using a magnetic bar in a nitrogen (N_2)-filled glove box overnight to ensure a homogeneous blended solution. In the application of a photosensor, blending the material is believed to alter the surface roughness of the thin film, increase light absorption, charge carrier generation and transport, and lead to enhancement in the OPD performance.

Aside from the organic solution, Poly (3,4-ethylenedioxy-thiophene)-poly(styrene sulfonate) (PEDOT:PSS) aqueous solution was also used. The PEDOT:PSS solution was purchased from H.C. Stark and filtered prior to use with a 0.45 μm syringe filter. PEDOT:PSS works effectively as a hole transport layer (HTL) by enhancing the performance of the device due to its advantages of having a higher work function compared to ITO. It helps to smoothen the ITO surface to enhance hole injection, facilitates hole transport and reduces the current leakage by preventing short-circuiting.

3.4 Fabrication process

The fabrication process of an OPD involves spin-coating of interlayer and organic materials and ends with vacuum deposition of Aluminium (Al) cathode. After the substrate was cleaned and prepared, an aqueous dispersion of PEDOT:PSS solution was spin-coated on top of the ITO substrate. The spin-coating of PEDOT:PSS was optimized

at 2000 rpm for 60 s to form a 40 nm thin film. Then, the substrate was transferred to the glove-box for the deposition of the photoactive layer. The photoactive material was spin-coated on top of the PEDOT:PSS layer at 2000 rpm for 30 s. The samples are subjected to thermal annealing to induce micro-phase separation of donor and acceptor material and improve the crystallization of thin film (Pei, Devi, & Subramani, 2014). After that, Al was thermally deposited on top of the photoactive layer in the Physical Vapour Deposition (PVD) chamber using a shadow mask to complete the fabrication process.

PVD is a process to produce metal vapour that can be deposited on electrically conductive material as a metal coating. The Al deposition was done under vacuum with a base pressure of about 10^{-4} mbar. Initially, Al was placed on a tungsten boat source that was capable of supplying sufficient heat to the Al by conducting the electricity. The current supplied will heat the tungsten boat and evaporate the Al onto the sample. Finally, the device was encapsulated using a glass lid and UV-cured epoxy to protect the materials from moisture and environmental contaminants. The whole process is summarized in Figure 3.2 below.

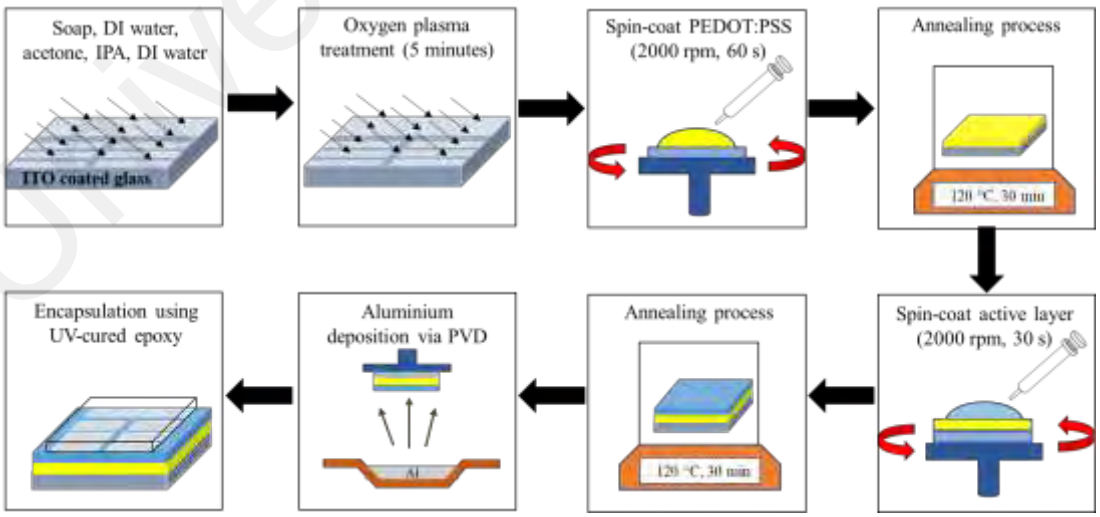

Figure 3.2: A flow chart showing steps involved in the fabrication process of an OPD device.

3.5 Characterization techniques

The properties of P3HT:OXCBA thin film were studied using several characterization techniques. The thickness of each deposited thin film layer was determined using KLA Tencor P-6 Surface Profilometer. UV-Vis spectroscopy was conducted to determine the light optical properties of the material. Aside from that, PL spectroscopy also allows us to estimate the charge transfer properties of the active material. Next, the morphology of the blend film was observed using AFM imaging. Then, the structural and elemental composition of the samples was also observed using Raman spectroscopy and XPS, respectively. UPS was also conducted as it gives the electronic structure of the material. Once the thin film is fabricated into a device, I-V and EQE measurements were carried out to investigate the electronic properties and performance of the device. Here, we present the working principle of the techniques that were briefly discussed in the following subtopics.

3.5.1 Surface Profilometer

A surface profilometer has been used to investigate the thickness of a sample film by scanning the height difference on the sample film. The image of the KLA Tencor P-6 profilometer used in this project is shown in Figure 3.3(a) and it can measure the roughness precision up to 0.1 nm. Prior to the characterization, the surface of the film was scratched to ensure abrupt surface steps that differentiate between the film layer and substrate. Next, the substrate was put on the stage and a diamond stylus was elevated down until it reached the surface of the sample. The diamond stylus could move laterally across the sample surface. The film's thickness was obtained by measuring the difference between the height of the thin film layer and substrate that were scanned across the film or at a specified distance. The deflection of the diamond stylus generates the thickness profile of the film's surface and gives the average thickness of the film.

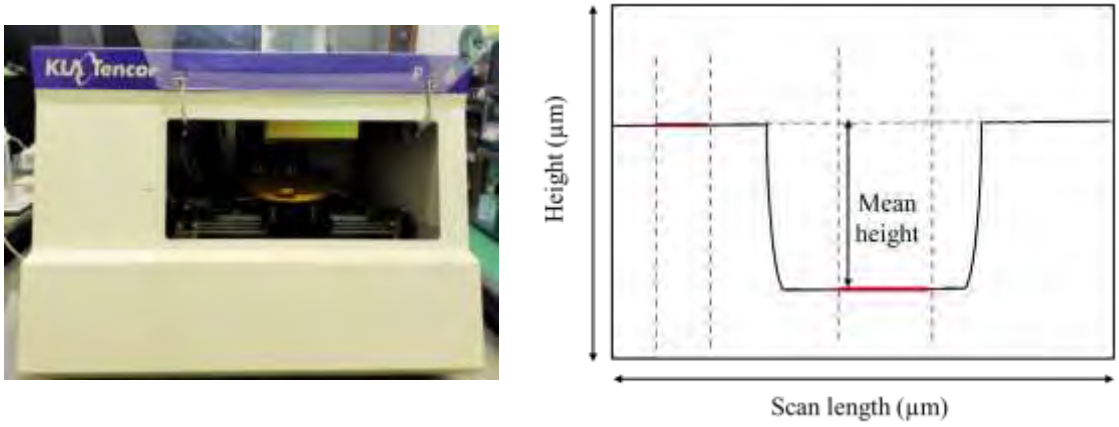

(a) (b)

Figure 3.3: (a) KLA Tencor P-6 Surface Profilometer and (b) the height profile image recorded by the profilometer.

3.5.2 X-ray Photoelectron Spectroscopy (XPS)

In this work, XPS is carried out for the quantitative study of the structural or chemical formation and identifying electronic information of the material at the sample surface. Basic XPS instrument requires a source of x-ray, an analyzer and a detector system. For instance, MgK and AlK radiation are normally used as a pass energy to create a monochromatic high energy x-ray excitation source of 1000-2000 eV that can penetrate the sample up to 10 nm depth. When the energetic x-ray photon bombards the surface of the sample, the atoms in the sample will absorb photons from the radiation and lead to ionization and emission of electrons from the inner shell of the atom. The ejected electron is known as a photoelectron. Then, an analyzer will analyze the electron energy and dispersed it based on their kinetic energy and will then be detected by a spectrometer. The emitted electrons have measured kinetic energy (KE) given as:

$$KE = h\nu - BE - \phi \quad \textbf{(3.1)}$$

where $h\nu$ is the photon energy used during the measurement, BE is the atomic orbital binding energy of the electron and ϕ is the work function of the spectrometer (Greczynski

& Hultman, 2020). In this study, a Thermo VG Scientific Alpha110 energy analyzer is used to detect the electrons.

XPS utilize the energy shift due to changes in the sample atom. It is known that the binding energy of a molecule is dependent on the orbital, the nucleus as well as the element from which it originated. Therefore, observing the value and intensity of the binding energy could identify the composition of elements present at the sample surface. In addition to that, binding energy also represents the electron density of the element. If the electronegativity is high, the atom's electron density is reduced, and the core level of the atom can be detected at higher binding energy. It also tends to be consistent with the oxidation state where higher oxidation exhibits a higher binding energy. These sensitivities make XPS very useful for identifying and measuring the chemical reaction that occurs on the sample surface.

Figure 3.4 shows a schematic of the XPS setup used in this work. This characterization technique was performed in an ultra-high vacuum (UHV) chamber equipped with a hemispherical analyzer and was using Al Kα source operating at 1486.6 eV. Firstly, the organic solution was spin-coated on a conductive ITO glass with a dimension of 1 cm^2 and the sample was fixed on a stainless-steel sample holder with a take-off angle of 90° prior to the characterization. The data obtained from this characterization is deconvoluted to show the specific chemical state of the element. The database for XPS measurement and specific binding energy of each element is provided by the National Institute of Standards and Technology (NIST).

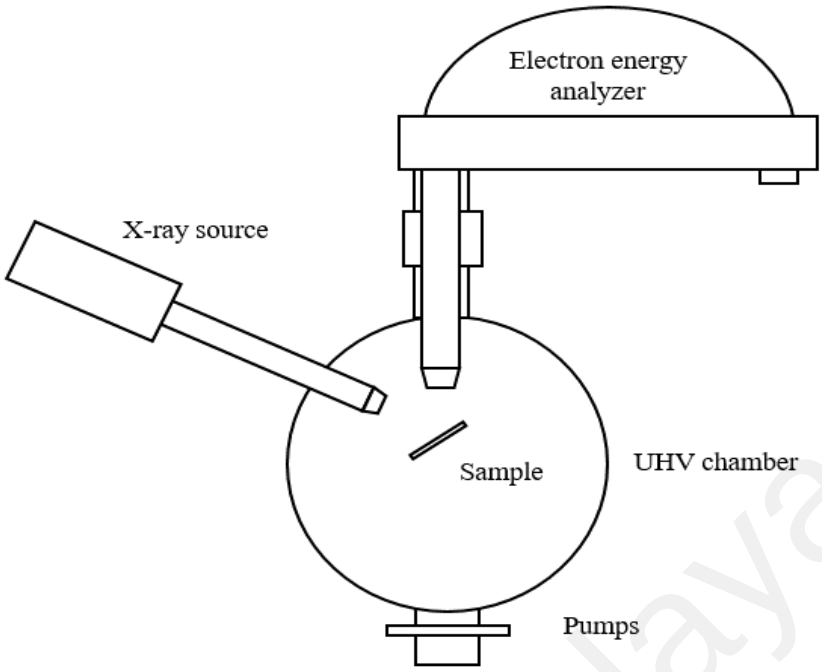

Figure 3.4: The schematic representation of XPS setup.

3.5.3 Ultraviolet Photoelectron Spectroscopy (UPS)

In contrast to XPS, UPS uses a gas discharge lamp to produce UV radiation in order to observe the valence level electrons. As only low energy source is used, this technique only penetrates the sample at an average of 2.5 nm depth and ionizes electrons at the most outermost orbital. Even though only a low energy irradiation source is adapted, the UV-photons exhibit higher photo-ionization cross-section with valence electrons compared to x-rays. The main features obtained from this technique are the work function and HOMO level measurement.

The sample used in this measurement is similar to the sample used in XPS analysis where an active solution was spin-coated on a conductive ITO glass to form a thin film. In this work, the binding energy of gold (Au) is used as a reference. The raw data is converted into binding energy via equation 3.1 and the results are illustrated as a function of binding energy relative to the Au. The HOMO level of the material can be determined by analyzing the UPS spectra using the following equations;

$$\phi = h\nu - \text{cut off energy} \quad \textbf{(3.2)}$$

$$\text{HOMO} = \phi + \text{HOMO}_{\text{onset}} \quad \textbf{(3.3)}$$

where cut off energy and value of $\text{HOMO}_{\text{onset}}$ are determined via linear extrapolation of the cut off energy region. (Helander, Greiner, Wang, & Lu, 2010; G.-H. Kim et al., 2013). Next, the LUMO energy level of the material can be estimated if the material band gap is known. The optical band gap (E_g) corresponds to the difference in the HOMO and LUMO level of a material. It can also be defined as the minimum energy required to excite an electron and can be calculated from UV-Vis absorption spectra using a simple equation:

$$E_g = \frac{1240}{\lambda} \quad \textbf{(3.4)}$$

where λ is the onset value of the absorption spectra at a longer wavelength as seen in Figure 3.5 below (Costa, Taveira, Lima, Mendes, & Santos, 2016). Then, the LUMO level can be estimated by subtracting E_g from the HOMO value.

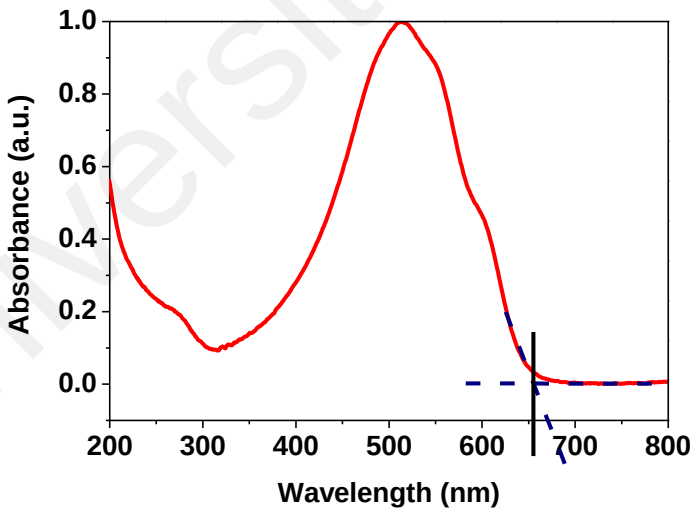

Figure 3.5: Example of onset value obtained from UV-Vis spectrum for the calculation of energy bandgap.

3.5.4 Light absorption spectroscopy

Absorption spectroscopy is an analysis measurement to study the interaction of light with a material. The quantity of light absorbed by a material is defined as:

$$A = \mathrm{Log}_{10} \frac{I_0}{I} \quad \textbf{(3.5)}$$

where A is the absorbance of a material, I_0 is the intensity of incident light and I is the intensity of transmitted light (Mayerhöfer, Mutschke, & Popp, 2016). This type of optical spectroscopy is known as UV-Vis spectroscopy. UV-Vis spectroscopy follows Beer Lambert's Law that states that the amount of light absorbed by a material is proportional to the concentration of the material. The amount of light absorbed by the material is presented in the absorbance spectrum.

Prior to the characterization, the organic solution was spin-coated onto quartz to form a thin film. Quartz has been used as a substrate as it helps probing the photo-absorption behaviour of the film at a lower optimal wavelength compared to glass. The sample in the form of thin film will be placed in a sample cell while a clean quartz will be placed in a reference cell. The basic schematic diagram of the UV-Vis setup is shown in Figure 3.6.

Light will be supplied through a monochromator and directed to the collimating lens which then would be dispersed into two identical light beams. One beam will pass through the sample cell and the other beam will pass through the reference cell. Then, a photodiode will measure the intensity of light that passes through the sample and reference cell, and amplifies the energy difference between the two cells. The energy difference between both cells corresponds to the amount of energy required to excite an electron from the ground state to a higher energy state and it corresponds to the wavelength of the absorbed light. Finally, the exact amount of light that passes through the sample will be processed and a software is used to construct the UV-Vis absorption spectrum.

In this work, a Perkin-Elmer Lambda 750 UV-Vis-NIR spectrometer and UV WinLab software are used to measure the optical absorbance of the material as a function of wavelength with a resolution of 1 nm.

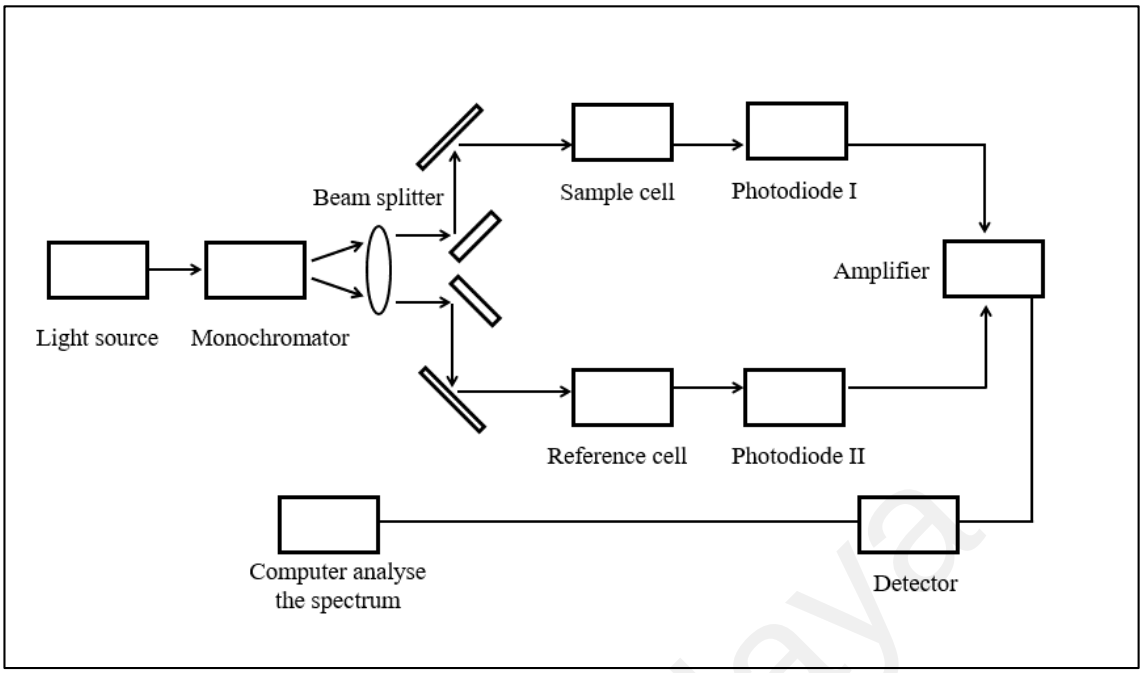

Figure 3.6: The schematic diagram of a UV-Vis spectroscopy system.

3.5.5 Photoluminescence (PL) Spectroscopy

PL is a nondestructive technique that uses spontaneous emission of light to analyze the electronic and optical transition of the material. The efficiency of PL measurement is determined by the wavelength and intensity of the excitation power source. An appropriate laser source needs to be chosen to avoid overlapping between excitation and emission spectra. In this work, the Renishaw inVia Raman Microscope is used at room temperature with a fixed excitation wavelength of 325 nm.

When a material absorbs sufficient energy from the source, electrons in the compound are excited to a higher energy. Usually, in order for excitation to occur, the excitation energy must have the same or greater energy than the difference between the initial and higher energy state. The excited electron will eventually fall back and recombine with hole, accompanied with energy lost in terms of the photon. In essence, PL measures the amount of photon radiated when an excited electron falls back to the ground state.

Observing the luminescence spectrum allows us to identify certain impurities of the film and estimates the carrier transfer and recombination in the film.

Figure 3.7 shows the typical operation setup for PL spectroscopy measurement. This measurement also uses samples in the form of thin film. The sample is placed in the centre of the sample holder and a light source was illuminated on the sample through the excitation monochromator. The laser beam passed through the small opening slits, travelled through the excitation filter before the incident on the sample. Here, photoluminescence occurs and photons are emitted for radiative recombination. The emission from the sample is then travelled into an emission monochromator before reaching a detector and then into a spectrometer. Finally, the computer interprets the data and the output signal emission spectrum is plotted with relative intensities against wavelength. Observing the luminescence spectrum allows us to identify certain impurities on the film and estimates the carrier transfer and recombination properties in the film.

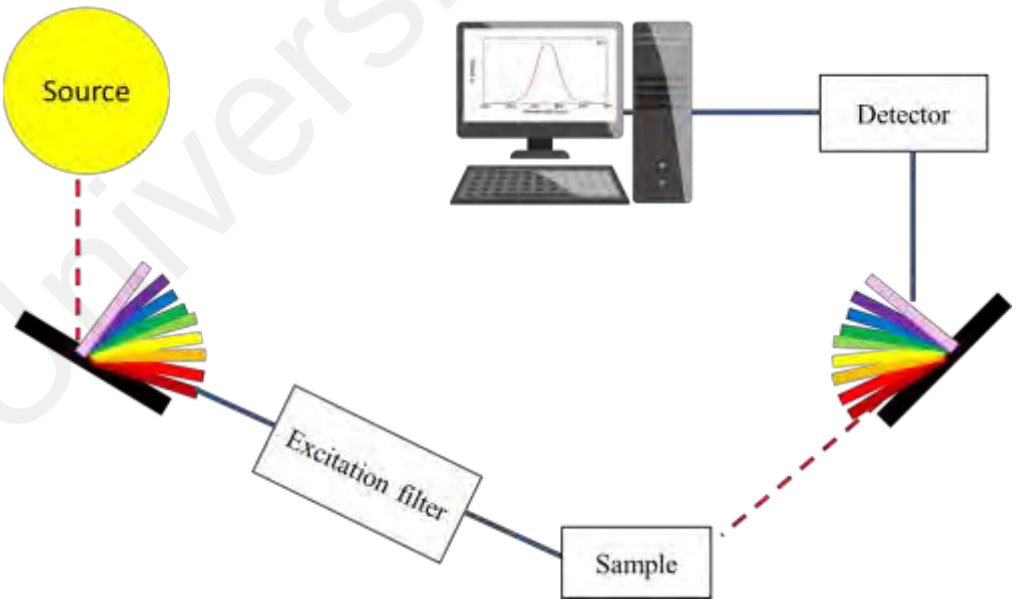

Figure 3.7: The schematic diagram of a PL spectroscopy system.

3.5.6 Atomic Force Microscopy (AFM)

AFM is a powerful surface imaging platform that can be used in scanning high resolution three-dimensional topographic images of a surface down to the scale of a nanometer. AFM can provide various surface measurement properties such as morphology, surface roughness and height profile of the sample surface. Prior to the fabrication, the sample was prepared by spin-coating an organic solution onto a glass substrate.

AFM operated by measuring the forces between a probe and a sample. As seen in Figure 3.8, the AFM instrument consists of a silicon-based cantilever with a sharp tip mounted on the end. For AFM imaging, the tip is brought into contact with the sample and scanned across the sample surface. As the tip approaches the surface, an attraction force between the tip and the sample surface causes the cantilever to deflect. When the probe passes over a bump on the surface, the cantilever has less room to oscillate and the oscillation amplitude decreases. On the other hand, the cantilever will have more space to oscillate when it passes over a depression, with an increase in the oscillation amplitude.

A feedback loop was used to ensure constant amplitude and force on the sample, and a position-sensitive detector was used to sense the motion of a cantilever. Variation in the amplitude of the sample surface is then measured by a detector and it is equivalent to the cantilever deflection.

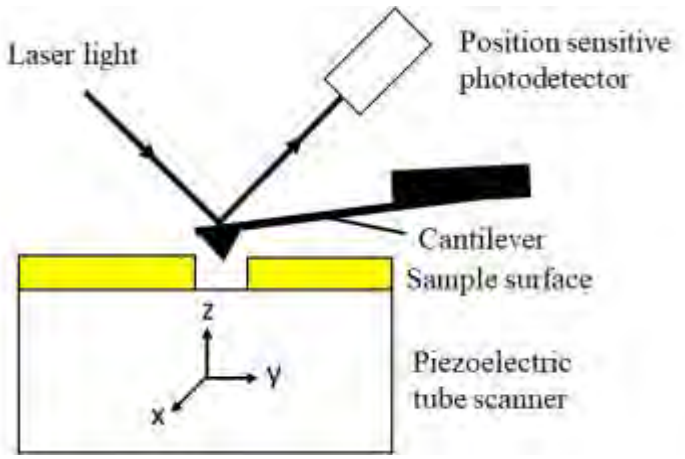

Figure 3.8: The schematic of AFM surface analysis operated in tapping mode.

3.5.7 RAMAN spectroscopy

Raman is a vibrational spectroscopic technique that uses the light scattering process to study the vibrational properties of a structure of a material. It relies on Rayleigh scattering theory and discusses vibrational properties of the bonds which include stretching, bending and rocking motion. Raman setup requires a monochromatic light source, diffraction grating as well as a detection system. The sample for this analysis was prepared in the form of a thin film that was coated on glass.

When a sample is exposed to a monochromatic light source, most of the light will be scattered at a similar wavelength as the light source. The scattered light will pass through a diffraction grating to separate them by their wavelength. Finally, a detection system will receive the signal and record the intensity of the signal at each wavelength. Then, a computer utilizes the signal and represents them in a graph. The spectrum identifies the type of bond present in the material. The schematic diagram of the Raman setup system is shown in Figure 3.9.

In this work, the characterization is carried out by using Renishaw inVia Raman Microscope. A laser with 325 nm excitation laser was employed and all spectra were taken in background configuration at room temperature.

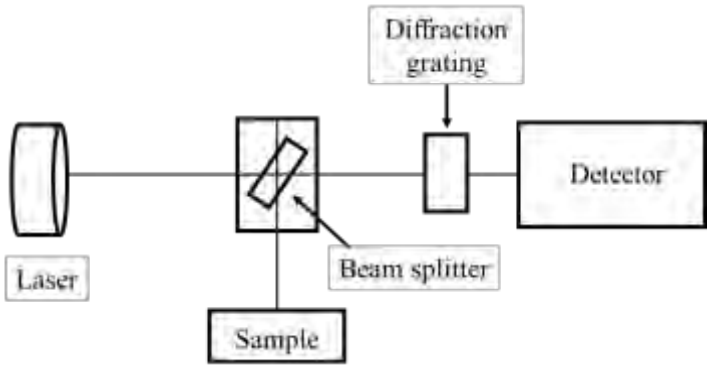

Figure 3.9: The schematic diagram of the Raman spectroscopy system.

3.5.8 Current-voltage (I-V) characterization

The performance of an OPD device is measured using the I-V characterization technique. This technique defines the performance of an OPD by giving out these key parameters; short-circuit current density (J_{sc}), photocurrent density (J_{ph}), and dark current density (J_d) of the device. J_{sc} is the amount of current that passes through the device when the voltage across the device is zero and J_{ph} is the amount of photocurrent measured across the device when bias is applied. On the other hand, J_d refers to the amount of current measured across samples in dark condition. These values yield information on charge transport properties in the cell as illustrated in Figure 3.11(a). In this characterization, the device was placed in a black box and subjected to an external bias voltage from Keithley 236 Source Meter Unit (SMU) which also used to simultaneously detect the current produced. An Air Mass 1.5 spectrum (AM 1.5G) with an intensity of 100 mA/cm^2 was used as the illumination source. This device represents sunlight with the sun at a zenith angle of 48.2° above the earth atmosphere. It also represents 1 sun value at the ambient temperature of 25 °C. This measurement is controlled using a Labview computer program.

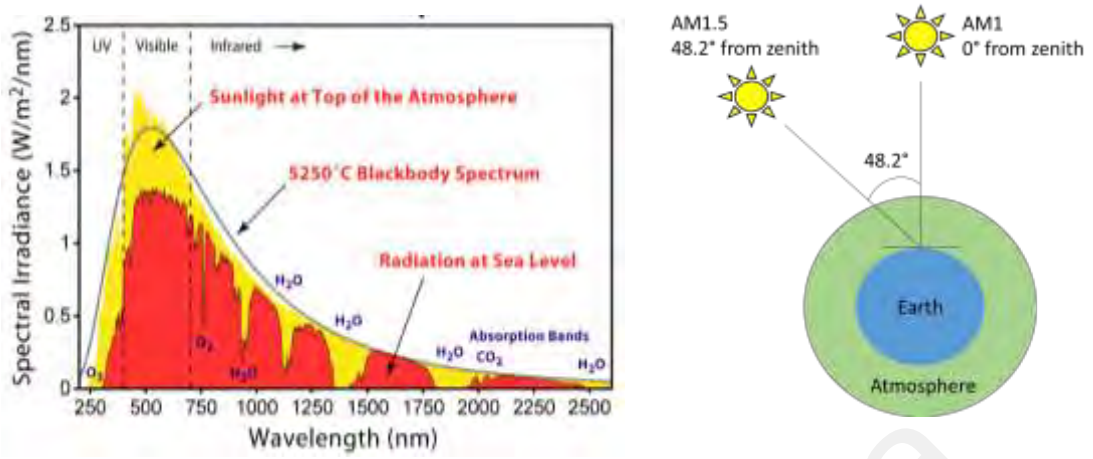

(a) (b)

Figure 3.10: (a) The AM 1.5 G radiation spectrum and (b) air masses at a different angle above the earth surface.

When an external bias is supplied, the charge will build up and the charge carriers will flow towards their respective electrodes. The difference in HOMO of donor and LUMO of acceptor will generate sufficient energy offset for the dissociation of electron and improve photocurrent generation.

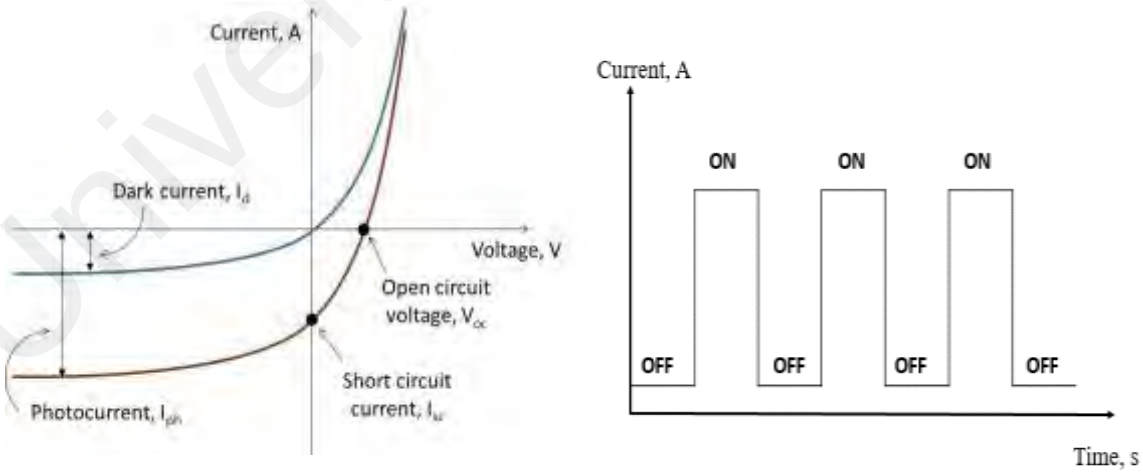

(a) (b)

Figure 3.11: The (a) I-V graph and (b) photoresponse behaviour of an OPD device obtained from I-V measurement.

In addition to that, responsivity (R) and specific detectivity (D*) of an OPD are also one of the important factors in determining the light-sensing abilities of a photodetector. R represents the magnitude of photocurrent generated at a certain power. It can also be calculated by the following expression:

$$\boldsymbol{R = \frac{J_{ph}}{P}} \quad \textbf{(3.6)}$$

where J_{ph} is the photocurrent density obtained from I-V characterization and P is the power of incident light intensity (An, Wang, & Xue, 2019). The photoresponse behaviour of the device can be observed by recording the rapid change in photocurrent as a function of time internal when light irradiated on the sample is controlled to be at 'ON' and 'OFF' states as illustrated in Figure 3.11(b). In this characterization, the time interval was set at 5 seconds to give sufficient energy for the sample to be stable.

Aside from that, the D* can be calculated using the equation:

$$\mathrm{D^*} = \frac{\boldsymbol{R}}{\sqrt{\boldsymbol{2qJ_d}}} \quad \textbf{(3.7)}$$

where q is an elementary charge (1.6×10^{-19} C) and J_d is the dark current density (An et al., 2019). As we can see in the equation above, high D* can be obtained by improving the responsivity and restraining the J_d (Liu, Lin, Liao, Wu, & Zheng, 2018).

In this work, each of the devices is fabricated by employing a binary blend solution of P3HT:OXCBA in conventional structure with stack order of ITO:PEDOT:PSS:P3HT:OXCBA:Al as shown in Figure 3.12. The devices are then tested in both dark and illumination condition.

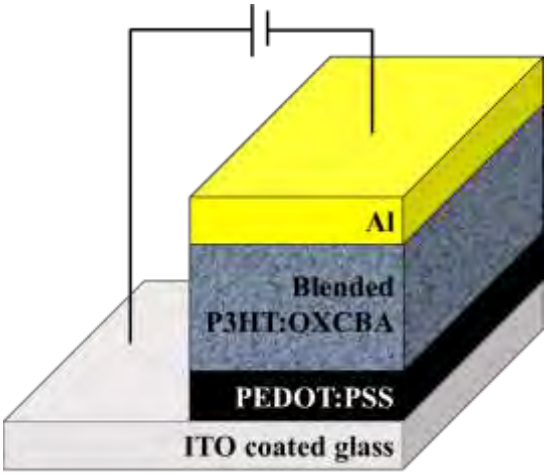

Figure 3.12. Schematic representation of stack order OPD device.

3.5.9 External Quantum Efficiency (EQE)

EQE measurement is carried out to measure the ability of the device to convert photons into an electrical signal. It is also defined as the conversion ratio between the number of electrons collected by the electrode and the incident photon. EQE is a critical indicator to evaluate the spectral response of the device. The EQE curve is typically plotted as a curve related to wavelengths. It can reflect the characteristics under various wavelengths which help to diagnose the performance of the device in order to improve the efficiency of the device. For instance, if 100 photons are irradiating on the surface of the device and only 80 electrons are generated, the EQE of the device is said to be 80%. This study utilizes Incident-Photon-to-Current Efficiency (IPCE) system with a 555 nm monochromatic laser source to measure the EQE of the device. This setup utilizes an optical power meter (Newport 1918-R) and monochromator illuminators (Newport Oriel Apex 70528 and Newport Oriel Connerstone 130 1/8 M monochromator). A laser with 555 nm wavelength was chosen as its light power would produce the maximum amount of light emitted per second compared to other wavelengths.

CHAPTER 4: RESULTS AND DISCUSSIONS

4.1 Introduction

It is well known that the mixture of materials could form percolating pathways for charge transport or traps depending on the energy level of the material. Hence, this chapter presents a detailed experimental study on the effect of blending different concentration ratios of material in OPD systems. This chapter also discusses the structural and chemical properties of the P3HT:OXCBA blends as well as their electrical performances. The correlation between optical and morphological properties of the film with OPD performance is investigated.

4.2 Thin Film Characteristics

4.2.1 Element Compositions

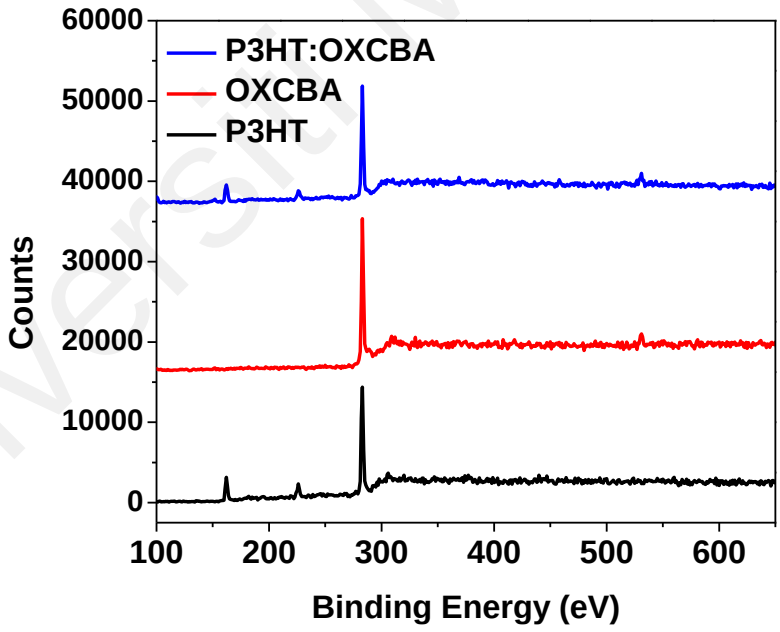

Figure 4.1: XPS survey spectrum for P3HT, OXCBA and P3HT:OXCBA thin films.

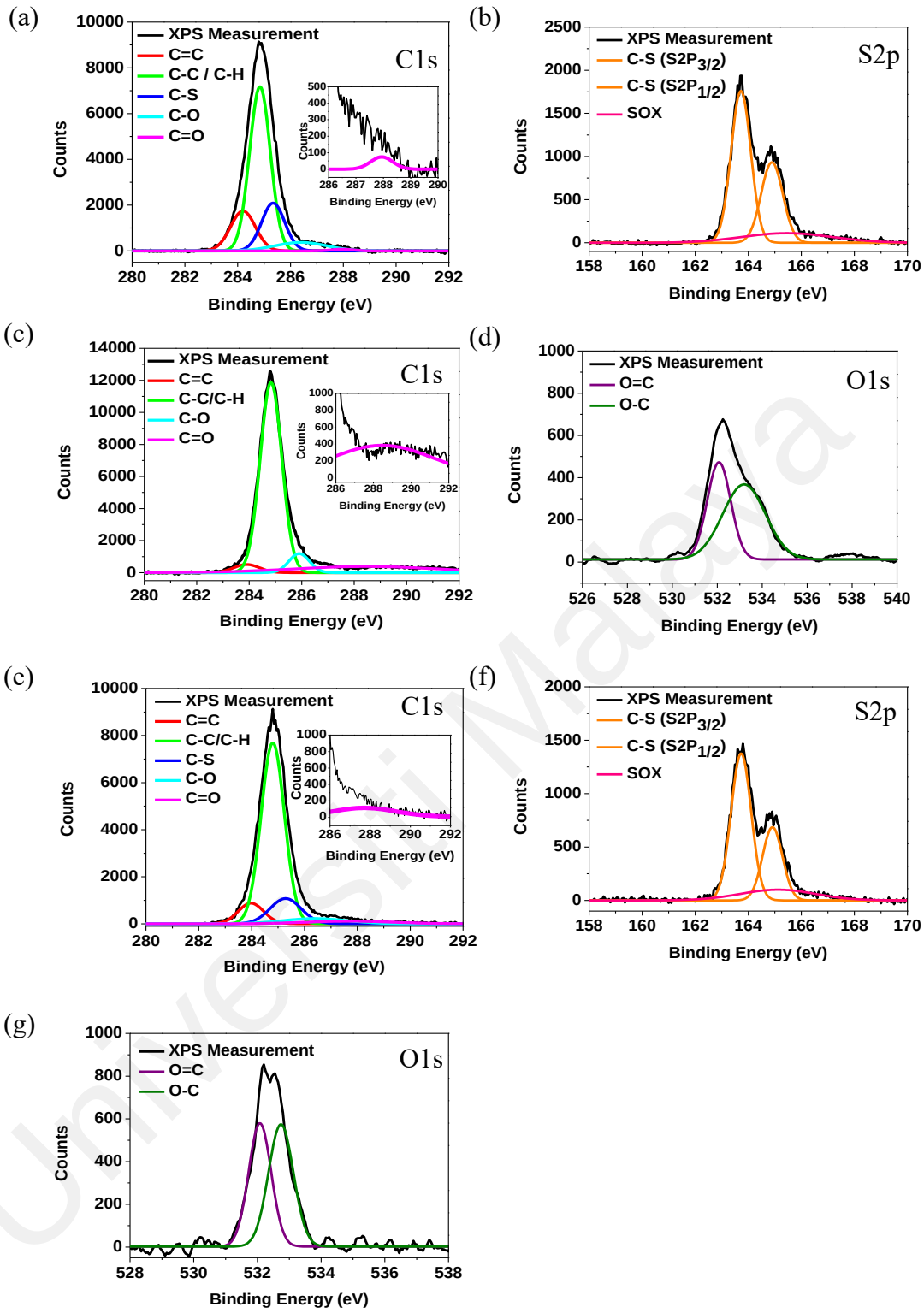

Figure 4.2: The XPS spectra of P3HT, OXCBA and P3HT:OXCBA composite thin film. (a) and (b) refer to C1s and S2p XPS spectra of P3HT, while (c) and (d) refer to C1s and O1s XPS spectra of OXCBA. On the other hand, (e), (f) and (g) are the XPS spectra for C1s, S2p and O1s of P3HT:OXCBA composite blend. The inset in C1s graphs shows the zoom image for C=O from 286 eV to 292 eV.

Table 4.1: XPS surface composition of P3HT, OXCBA and P3HT:OXCBA thin films obtained from wide scan analysis.

	C (%)	S (%)	O (%)
P3HT	81.86	18.14	-
OXCBA	88.32	-	11.68
P3HT:OXCBA	72.42	15.53	12.06

In brief, the structure of P3HT is made up of carbon, hydrogen and sulphur, while OXCBA only comprises carbon and hydrogen. In this XPS characterization, however, hydrogen is excluded due to the detection limit of XPS. Table 4.1 shows XPS survey spectra for P3HT, OXCBA and P3HT:OXCBA thin films. Table 4.1 gives the elemental composition for the thin films along with oxygen content found on each film. In addition to that, Figure 4.2(a)-(g) shows the XPS spectra of P3HT, OXCBA and their composite thin films. All XPS spectra are calibrated with adventitious C1s carbon peak at 248.8 eV with an error of approximately 1.7 eV due to the variation on the work function of the samples and the deconvolution of each chemical binding state is carried out using Gaussian curve fitting.

Based on the chemical structure of P3HT and OXCBA, no oxygen should be present to avoid oxidation of the sample. However, there is a small amount of oxygen detected suggesting oxidation of the material during the sample preparation or while transferring the samples into the XPS system. From the XPS analysis, P3HT thin film mainly consisted of carbon and sulphur with low peaks of oxygen. It can be observed in Figure 4.2(a) that there is a strong and defined peak at 284.8 eV in the C1s spectrum of P3HT thin film, corresponding to the C-C and C-H bond of its main structure. Other symmetric peaks are also observed at 284.0 eV (C=C), 285.5 eV (C-S), 286.3 eV (C-O) and 287.8 eV (C=O). The sulphur content from the S2p core-line spectrum (Figure 4.2(b)) presented a doublet at 164.0 eV and 165.0 eV that attribute to the C-S bond in the thiophene ring,

and the shake-up structure on the higher binding energy of C1s and S2p spectrum indicates that the π-conjugated system of P3HT is broken. However, as the oxygen contamination is low, the O1s scan did not give a defined peak which indicates there is insignificant oxidation in the P3HT polymer.

On the other hand, the oxygen content in OXCBA thin film was found to be at 11.68 %. The increase in C-O and C=O peak at 532.0 eV and 533.0 eV from O1s spectra of OXCBA thin film may be due to the breaking of fullerene (C_{60}) cage and oxidation of carbon atoms. From closer observation on the P3HT:OXCBA composite thin film (Figure 4.2(f)), it is clear that sulphur distribution was reduced compared to P3HT thin film while the oxygen contents are found to be higher compared to OXCBA thin film. This may suggest that sulphur in P3HT:OXCBA thin film is more exposed to oxidation compared to P3HT thin films along with the oxidation of carbon atoms from P3HT and OXCBA molecules.

4.2.2 Absorption Characteristic of the Active Layer

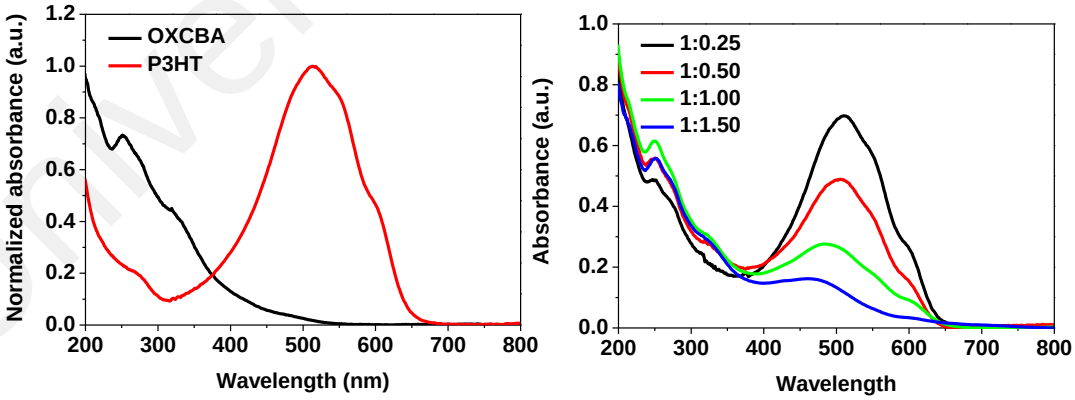

(a) (b)

Figure 4.3: Absorption spectrum for (a) P3HT and OXCBA, respectively and (b) P3HT:OXCBA blend film with the ratio of OXCBA ranging from 0.25 to 1.50 with respect to P3HT.

The ability of an active layer to absorb light is important in the application of a photodetector. As shown in Figure 4.3(a), OXCBA appeared to have greater light

absorbance at the lower wavelength region (UV regime) with a shoulder at 251 nm, while P3HT reveals a significant peak at 514 nm along with a vibronic peak at 600 nm which represents the vibrational excitation due to highly ordered P3HT chain structure. However, there is less light absorption especially at the valley around 250-400 nm. Therefore, the two materials are combined to broaden the absorption bandwidth of the photoactive layer and enhance the absorptivity of the photoactive layer for the whole visible region.

It is evident from Figure 4.3(b) that the valley diminished when the concentration of OXCBA is getting higher in the composition. Absorption spectra of P3HT:OXCBA thin films show absorption bandwidth in the range of 300 to 650 nm for all ratios. The absorption in the lower region increases with an increase in the concentration of OXCBA but it significantly affects the peak of P3HT at 510 nm which has seen the blue-shift behaviour. Since the concentrations of P3HT are fixed throughout this work, the quenching at the peak of the P3HT fraction can be attributed to the interaction between the P3HT molecule and OXCBA. However, the peak is red-shifted in P3HT:OXCBA thin film of 1:0.50 ratio, which shows the broadest absorption region. The redshift can be explained by the increase in charge transfer polarizability which is indicative of the increase in delocalization and also increase in the dielectric constant of the blended film (Bernardo et al., 2014; Brebels, Manca, Lutsen, Vanderzande, & Maes, 2017).

It can also be observed from Figure 4.3(b) that the shoulder at 600 nm diminished with the increase in OXCBA concentration. Therefore, we suggest that the concentration of OXCBA is responsible for the degree of P3HT packing in P3HT:OXCBA blended films. Due to their different molecular size, OXCBA will fill the void in the P3HT chain structure which will lead to a higher degree molecular order of the blended film and affect the light-harvesting properties of the blended film. Eastham et al. has reported that optical

absorption corresponds to the morphology of the blend that might be due to optimal phase separation between donor and acceptor material and increase in π–system delocalization due to the increase in crystallinity. Zhokavets et al. also reported that optical absorption increases linearly with the increases in crystallinity (Eastham et al., 2017; Zhokhavets, Erb, Gobsch, Al-Ibrahim, & Ambacher, 2006). This could explain the absorption trend in lower regions where light absorption increases with an increase in OXCBA incorporation up to ratio 1:1.00.

However further increase in the OXCBA ratio could result in the diffusion of OXCBA out of the polymer matrix, resulting in higher surface roughness and lower crystallinity of the blend when the OXCBA ratio was increased to 1.50. Niu et al. also reported that absorptivity will decrease along with increasing in spacing distance between two peaks and higher intersection angle (rougher surface) as the light wave that incident on the surface will be reflected (Niu, Zhu, & Lv, 2019).

4.2.3 HOMO and LUMO Levels

Next, UPS analysis was carried out to determine the energy level of the materials before fabricating an OPD device. This was done to ensure proper cascade energy alignment for efficient carrier transport. Figure 4.4 shows the UPS spectra obtained from the analysis and the calculated HOMO level for P3HT and OXCBA are summarized in Table 4.2. Basically, the E_g value corresponds to the difference between the HOMO and LUMO level of the material. From the E_g value obtained from UV-Vis, we are able to estimate the LUMO level of the thin films by subtracting the E_g from the HOMO energy level.

The calculated HOMO level obtained from UPS is 4.94 eV and 5.66 eV for P3HT and OXCBA, respectively. Therefore, the LUMO level of P3HT and OXCBA were determined to be 3.07 eV and 3.47 eV, respectively. The alignment of energy levels

obtained for P3HT and OXCBA can be seen in Figure 4.5, while the energy levels for ITO, PEDOT:PSS and Al are obtained from literature.

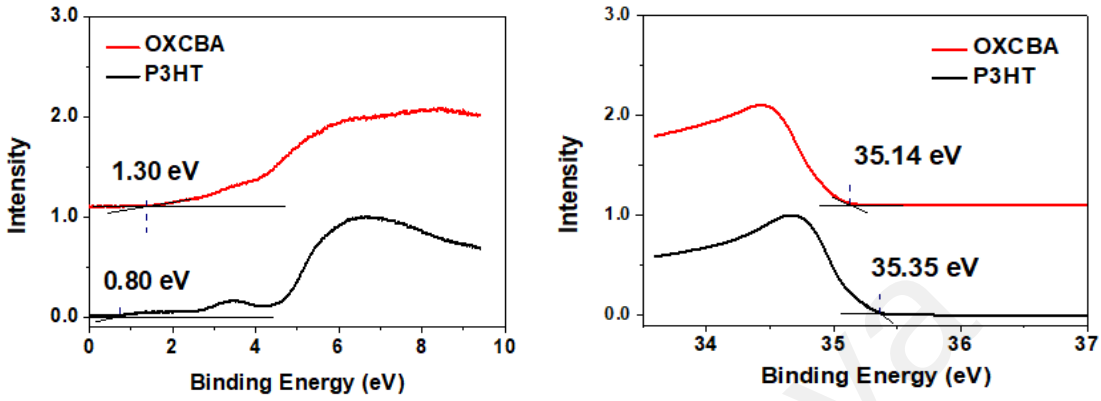

(a) (b)

Figure 4.4: UPS spectra and representation of (a) $HOMO_{onset}$ and (b) cut off energy value for the determination of work function and HOMO level of the material.

Table 4.2: Calculated HOMO and LUMO level of P3HT, OXCBA and P3HT:OXCBA blended thin films.

	$HOMO_{onset}$ (eV)	Cut-off energy (eV)	Work Function (eV)	HOMO level (eV)	E_g (eV)	LUMO level (eV)
P3HT	0.80	35.35	4.15	4.94	1.87	3.07
OXCBA	1.30	35.14	4.36	5.66	2.19	3.47

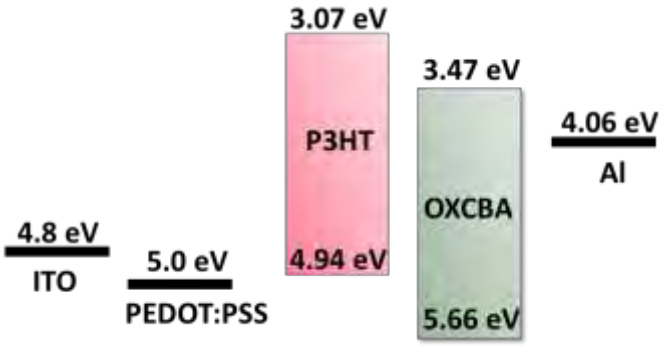

Figure 4.5: The cascade energy levels alignment of P3HT:OXCBA OPD device.

Table 4.3 has listed the HOMO and LUMO energy level of P3HT and OXCBA obtained from literature and present study using photon spectroscopy and electrochemical

techniques. Cyclic-voltammetry (CV) is an electrochemical technique that is commonly used to estimate the ionization potential and electron affinity of a material as it is significantly cheaper and simpler. However, CV-estimated data depends on the type of material and the data point has the potential to deviate due to difference in polarization energy or solvation energy of the thin film to the solution, thus making the data to be less accurate in the determination of ionized energy level.

On the other hand, UPS could give a precise estimation of the ionization potential of the thin film compared to CV-measured data as it was carried out in vacuum. The measurement in CV and UPS may differ due to the difference in calibration technique, experimental setting, type of sample and data analysis method.

Table 4.3: Comparison of HOMO and LUMO level obtained from literature.

Material	Measurement	HOMO level (eV)	LUMO level (eV)	References
OXCBA	CV	-	3.66	(K.-H. Kim et al., 2011)
	CV	-	3.65	(K.-H. Kim et al., 2012)
	CV	-	3.66	(H. Kang et al., 2013)
	UPS	5.66	3.47	Present
P3HT	EIS	5.27	3.79	(Acevedo-Peña, Baray-Calderón, Hu, González, & Ugalde-Saldivar, 2017)
	CV	5.22	3.68	(Acevedo-Peña et al., 2017)
	CV	5.12	2.84	(Tremel & Ludwigs, 2014)
	UPS & IPES	4.65	2.13	(Guan, Bok Kim, Loo, & Kahn, 2011)
	UPS	4.94	3.08	Present

4.2.4 Electrical Performance of OPDs

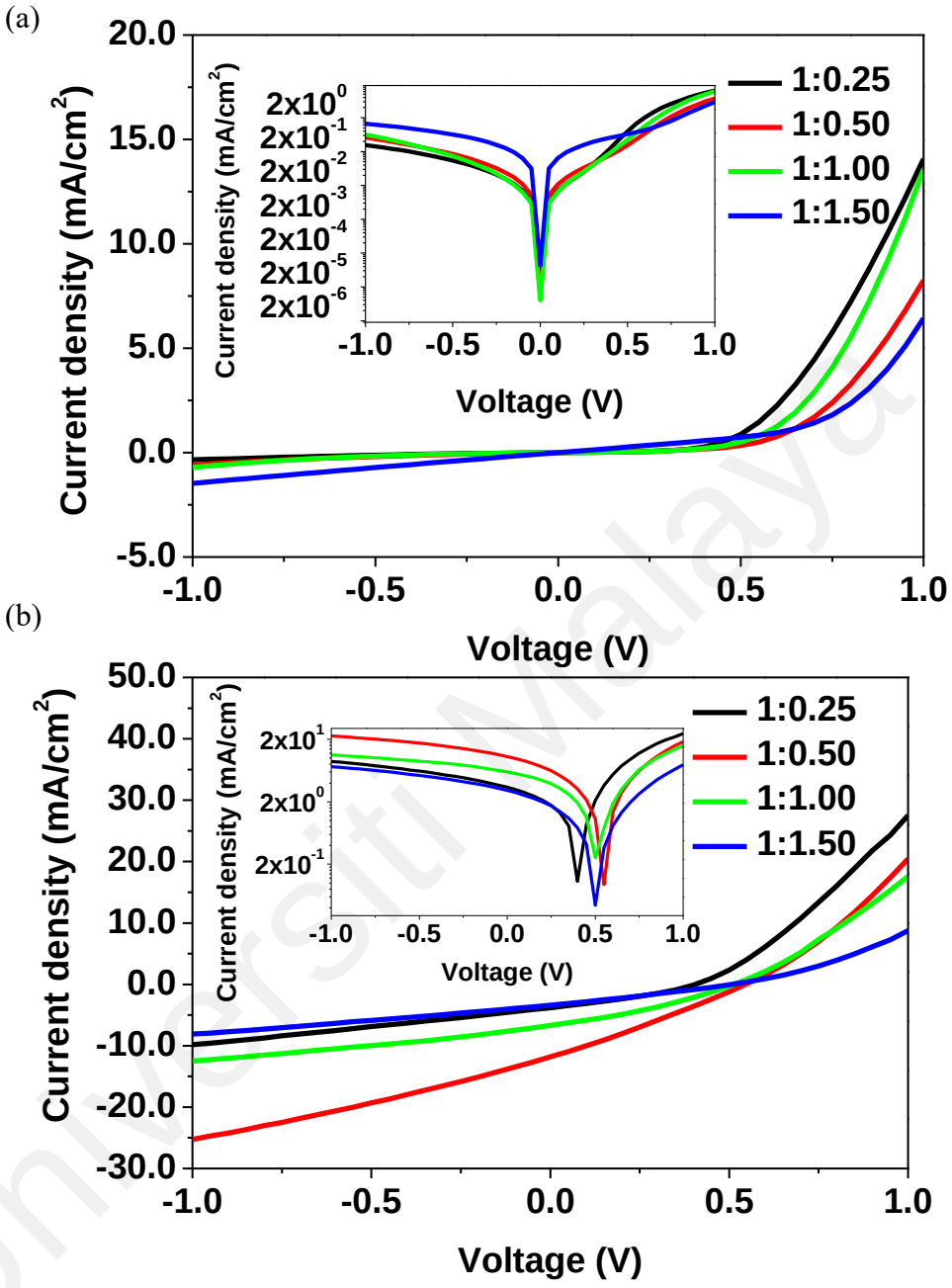

Figure 4.6: The J-V graph of P3HT:OXCBA devices characterized in (a) dark and (b) light environment. The inset shows a semi-log graph of the J-V where the x-axis is plotted in linear mode while the y-axis is in log mode.

Further, the I-V characterization of four different P3HT:OXCBA devices have been carried out to elucidate the relationship between different concentrations of small molecule fullerene derivatives, OXCBA with respect to the P3HT and their photo-sensing performance. The performance of the devices along with their response behaviour upon

irradiation of light under -1 V is summarized in Table 4.4. According to Table 4.4, the J_{ph} value of the fabricated devices increases from 9.84 mA/cm^2 at the ratio of 1:0.25 to 25.27 mA/cm^2 at the ratio of 1:0.50. It is shown that a small increase in the ratio of OXCBA from 0.25 to 0.50 results in an increase in J_{ph} value. However, as the concentration of OXCBA increases further, the J_{ph} value decreases to 12.48 mA/cm^2 and finally 8.09 mA/cm^2. This agrees with the discussion that OXCBA might diffuse out of the matrix at a higher concentration, leading to poorer morphology and lowering the performance of the device.

Figure 4.6(a) also reveals that J_d increases with the increases in OXCBA concentration. This supports the existing electron channel condition between electrodes and interfaces of photoactive layers. More leakage current will occur with higher composition of n-type material (OXCBA). As seen in Table 4.4, J_d increases by four times at the highest ratio of 1:1.5, but the value is still within acceptable range if compared with values reported by others (Abdullah et al., 2018; Ahmad, Abdullah, & Sulaiman, 2013; Ji et al., 2019; C.-C. Lee et al., 2019).

Table 4.4: Photosensing characteristics of P3HT:OXCBA devices of different ratios at -1 V.

P3HT: OXCBA ratio	J_{ph} (mA/cm^2)	J_d (mA/cm^2)	Rise Time (ms)	Decay Time (ms)	ON/ OFF ratio	R (mA/W)	D* (x10^{10} Jones)
1:0.25	9.84	0.35	445	363	28.30	98.37	0.93
1:0.50	25.27	0.58	445	309	43.40	252.69	1.85
1:1.00	12.48	0.71	445	336	17.51	124.78	0.83
1:1.50	8.09	1.47	-	-	5.50	80.92	0.37

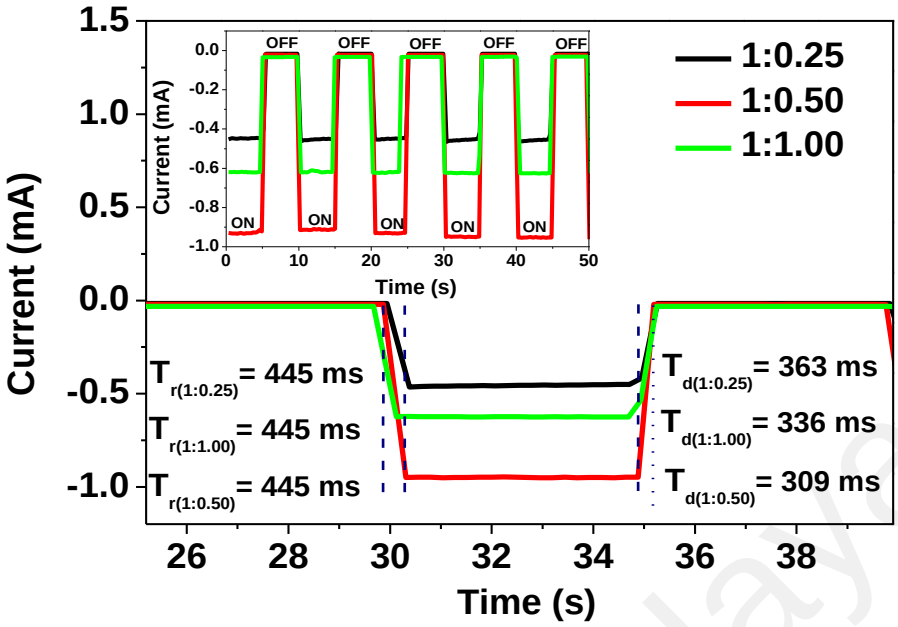

Figure 4.7: Photoresponse behaviour of P3HT:OXCBA OPD devices.

Figure 4.7 illustrates the photoresponse behaviour of the photodetector under -1 V bias voltage. It reveals that the devices exhibit consistent response, good repeatability and rapid change of states. The rise time (time for which device response rises from 10 to 90%) and decay time (time for which the device response fall from 90 to 10%) of P3HT:OXCBA device with the ratio of 1:0.50 is determined to be ~445 ms and ~309 ms, respectively, which is the fastest decay time among all devices with highest photocurrent gain ratio (ON/OFF state) of 4.34 x 10^1.

The device with ratio of 1:0.50 also shows the maximum responsivity of 252.69 mA/W compared to other devices (ratio 1:0.25 = 98.37 mA/W, ratio 1:1.00 = 124.78 mA/W and ratio 1:1.50 = 80.92 mA/W). Apart from that, the D* obtained for ratio 1:0.50 is 1.85 x 10^{10} Jones, and it is the highest detection limit observed among the devices. On the other hand, OPD device with a ratio of 1:1.50 has the least performance and the photoresponse behaviour of the device is not included in Figure 4.7 since the device is unstable.

Therefore, it is suggested that the blend ratio of 1:0.50 exhibits the best OPD performance while the ratio 1:1.50 shows the worst performance.

Table 4.5: Comparison of J_{sc} and R between literature and present study of P3HT:OXCBA devices at 0 V.

Active Layer	J_{sc} (mA/cm^2)	R (A/W)	References
P3HT:OXCBA	10.32	103.20	(H. Kang et al., 2013)
P3HT:OXCBA	10.30	103.00	(K.-H. Kim et al., 2011)
M-OXCBA	9.85	98.50	(H. Kim et al., 2015)
DM-OXCBA	10.52	105.20	(H. Kim et al., 2015)
P3HT:OXCBA	9.78	97.80	(K.-H. Kim et al., 2012)
P3HT:TMX_OXCBA	7.22	72.20	(H. Kim et al., 2016)
P3HT:OXCBA	11.82	118.16	Present work

Generally, J_{sc} value is correlated with the amount of light absorbed by the active layer and it is directly proportional to the device responsivity measured at 0 V. Results in Table 4.5 shows that the J_{sc} value obtained in this work has exceeded others. It is notable that the device follows the conventional structure of a photodiode and the electron transport layer is not employed in the fabrication, while other reported devices follow the inverted structure with the addition of LiF as the electron transport layer. In addition to that, the plasma etching treatment that was carried out at ITO before the fabrication process also contributes to the higher performance of the devices. The treatment helps to improve the adhesion between the spin-coated layer and the ITO and ensure smooth coating. Therefore, it can be deduced that this fabrication process could still provide comparable performances with easier process and its performances could be enhanced.

4.2.5 Photoluminescence Measurement

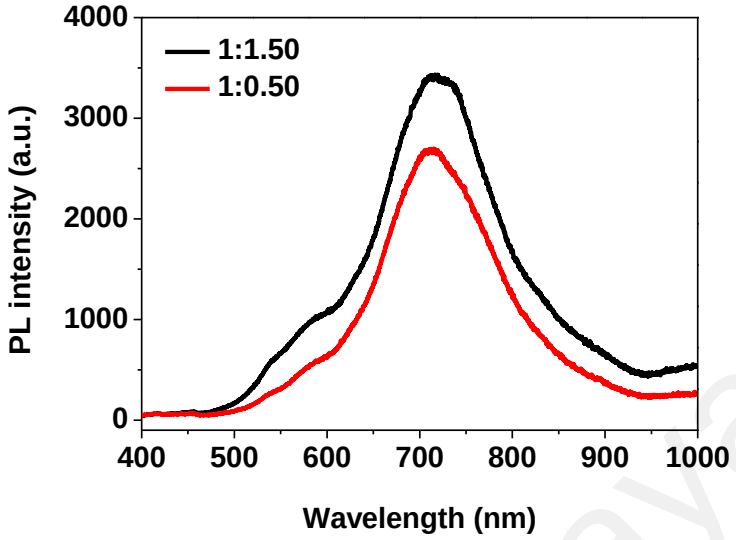

Figure 4.8: PL spectra of P3HT:OXCBA thin film with ratio 1:0.50 and 1:1.50.

Next, PL analysis was carried out to study the charge transport behaviour in the blended film. Two blend ratio, 1:0.50 and 1:1.50 was chosen to compare the electroluminescence properties between the best and the worst performance of P3HT:OXCBA OPDs. Figure 4.8 elucidates the PL spectra in the range of 400 to 1000 nm obtained with an excitation wavelength of 325 nm. It can be observed that PL spectra of P3HT:OXCBA thin films show peak emission at 712 nm and a shoulder around 604 nm which corresponds to the vibronic peak of the molecules. The PL spectrum of ratio 1:1.50 shows the highest peak while the peak for ratio 1:0.50 is significantly quenched by 22% relative to the peak of 1:1.50 blended ratio. As PL measures the number of photons that are radiated due to recombination of charge carriers, this highly quenching efficiency of PL peak suggests less recombination and a better chance for charge transfer mechanism in the blend film.

In addition to that, the Stokes shift between absorption and emission peak was also observed. Figure 4.9 possesses a normalized absorption and emission spectra for P3HT:OXCBA blends with ratio 1:0.50 and 1:1.50. Upon photo-absorption of light, the

molecules undergo distortion or structural reorganization to adopt a more regular structure and stabilize the excited state, followed by a red-shift in emission (Itskos et al., 2011). The difference in the ground and excited state photon energy is known as stoke shift. As seen in Figure 4.9, blend film with a ratio of 1:0.50 has a smaller stoke shift compared to 1:1.50. Yanfei Xu et al. has reported that the smaller stoke shift suggests more regioregular arrangement and less regiorandom structure in the ground state, whereas larger stoke shift will have more regiorandom structure (Y. Xu et al., 2018). Therefore, we can also assume that the P3HT:OXCBA blend with a ratio of 1:0.50 provides better surface morphology compared to 1:1.50 thin film.

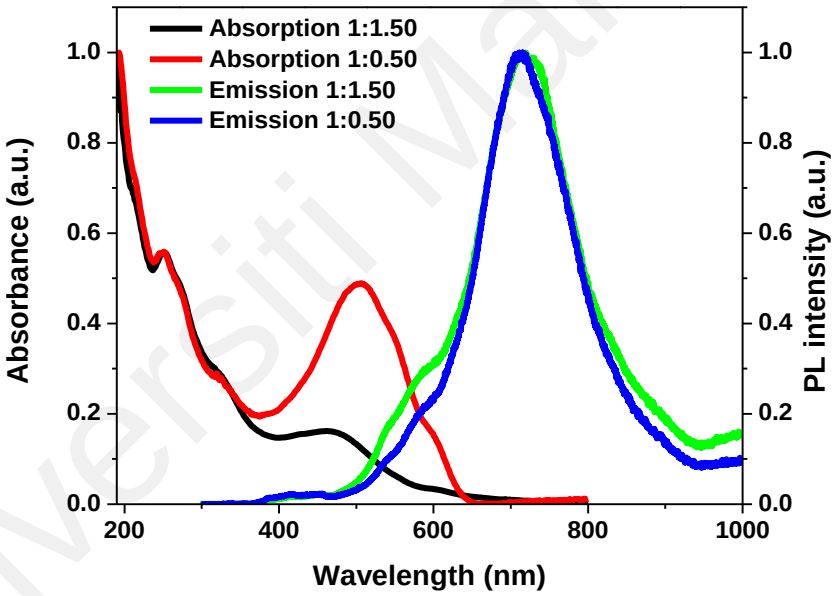

Figure 4.9: Normalized absorption and emission spectra for blend ratio 1:0.50 and 1:1.50.

4.2.6 Molecular Vibration Modes

For the further study of the molecular vibration modes in P3HT:OXCBA blended thin film, Raman spectroscopy is conducted in the range of 0 to 3200 cm^{-1} using a 325 nm laser source. Raman spectra of P3HT, OXCBA and P3HT:OXCBA composite blend film seen in Figure 4.10 features all vibrational modes as reported in literature that includes vibration, stretching and band bending with intensity varying from low to high values.

All peaks are summarized in Table 4.6. It is observed, mainly in P3HT:OXCBA (1:1.50), that there are small peaks occurring at 579 cm^{-1} to 780 cm^{-1} which correspond to C-H out of phase bending. From literature, the peak at 728 cm^{-1} is also said to be associated with the rocking vibration of the C-S-C thiophene ring of P3HT.

According to the literature, the C-H in phase vibrations peak that is observed at 1090 cm^{-1} is not from the P3HT molecule, hence this vibration peak may come from the OXCBA molecule and the difference in intensity may be due to the interaction of OXCBA with the P3HT molecule. As seen in Figure 4.10(c), the intensity for a peak at 1091 cm^{-1} for ratio 1:1.50 is higher compared to the peak in the 1:0.50 blend. This suggests that there is more interaction between OXCBA and the P3HT molecule as the concentration of OXCBA is higher in the 1:1.50 blend. From Figure 4.10, the band also yield some peaks appearing 1378 cm^{-1}, 1450 cm^{-1} and 1509 cm^{-1} that are related to asymmetric C=C skeletal stretching deformation, symmetric C=C stretching ring vibration and asymmetric C=C stretching vibration that come from P3HT and OXCBA fraction, while the peaks at the range of 2895 cm^{-1} to 2927 cm^{-1} are assigned to symmetric and asymmetric C-H deformation vibration of $–CH_2–$ and $–CH_3–$ moieties (Wei, Scudiero, & Eilers, 2009).

The Raman shift is the energy difference between incident and scattered light. When light comes in contact with the material, it will either gain or lose some quanta by interacting with the phonon. The energy of the phonon is determined by the amount of shift. If atomic bonding between molecules is considered as spring, the vibration energy will be lower for longer bond length, and the vibration energy is higher for shorter bond length. Therefore, for low energy phonons, the peak will be shifted towards a lower wavenumber whereas the peak will shift towards a higher wavenumber for a high energy

phonon. The downward shift in the wavenumber also indicates more ordered structure of P3HT:OXCBA blend film and the conjugation length of the blend is enhanced.

Although some of the peaks in the OXCBA fraction closely resemble the peaks in P3HT:OXCBA blend film, the intensity between the Raman modes greatly differ and the peaks that are attributable for the OXCBA fraction are not observed clearly. This suggests that the molecular structure of the blend film is dominated by P3HT and the influence of OXCBA are almost negligible.

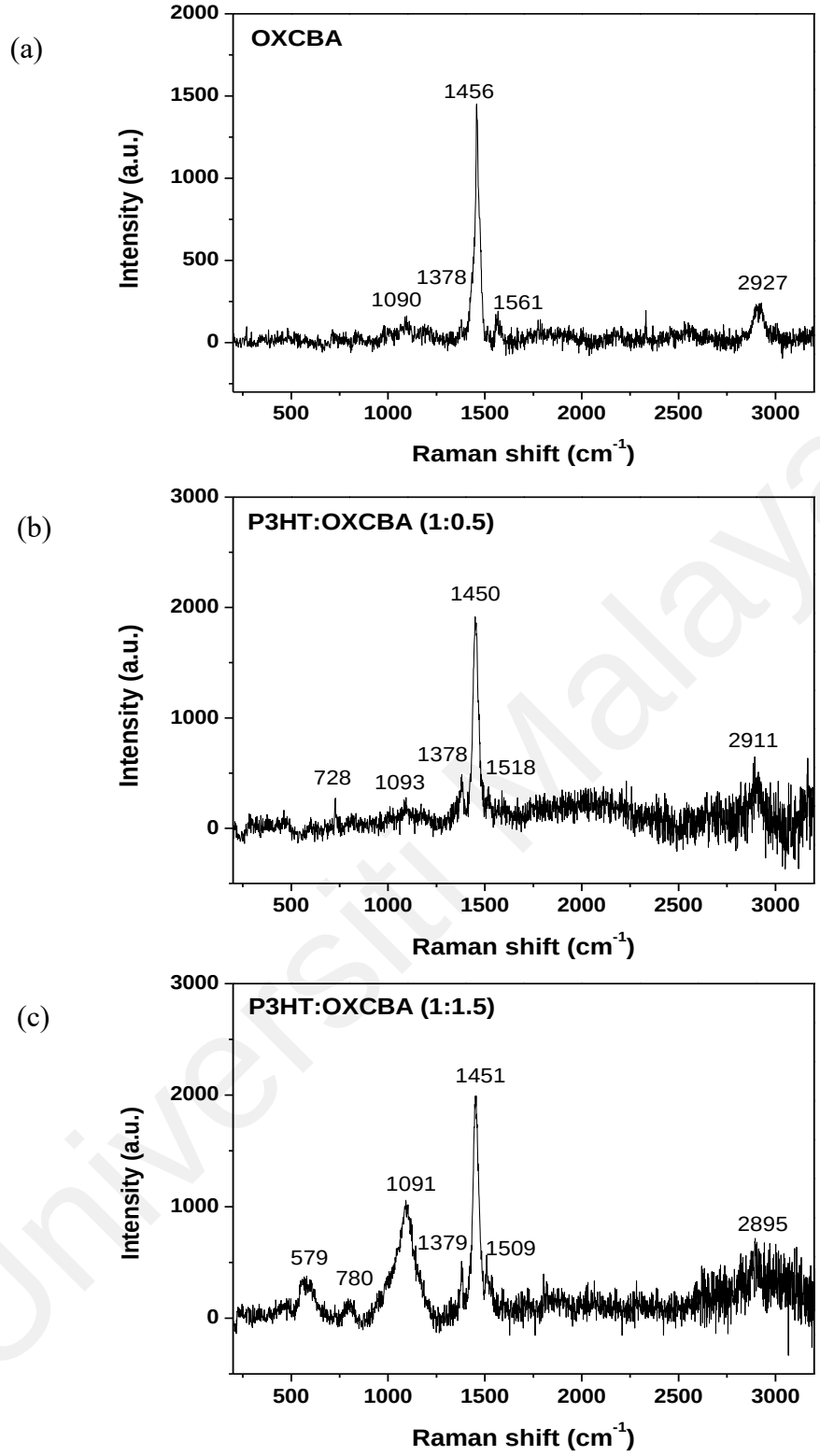

Figure 4.10: Raman spectra of (a) OXCBA and P3HT:OXCBA thin films with the ratio of (b) 1:0.50 and (c) 1:1.50.

Table 4.6: Observed Raman shifts (cm^{-1}) of OXCBA and P3HT:OXCBA blended thin films.

OXCBA	P3HT:OXCBA (1:0.50)	P3HT:OXCBA (1:1.50)	Approximate description of vibrations
-	-	579	$C\text{-}H_{ring\text{-}deformation}$
-	728	780	$C\text{-}S\text{-}C_{ring\text{-}deformation}$
1090	1093	1091	$C\text{-}H_{bending}$
1378	1378	1379	$C{=}C_{streching}$
1456	1450	1451	$C{=}C_{streching}$
1561	1518	1509	$C{=}C_{streching}$
2927	2911	2895	$C\text{-}H_{stretching}$

4.2.7 Surface Roughness

To prove the correlation between the morphology of the active layer and their performance, we performed an AFM analysis that operates in tapping mode in order to examine the morphology and surface roughness of the film.

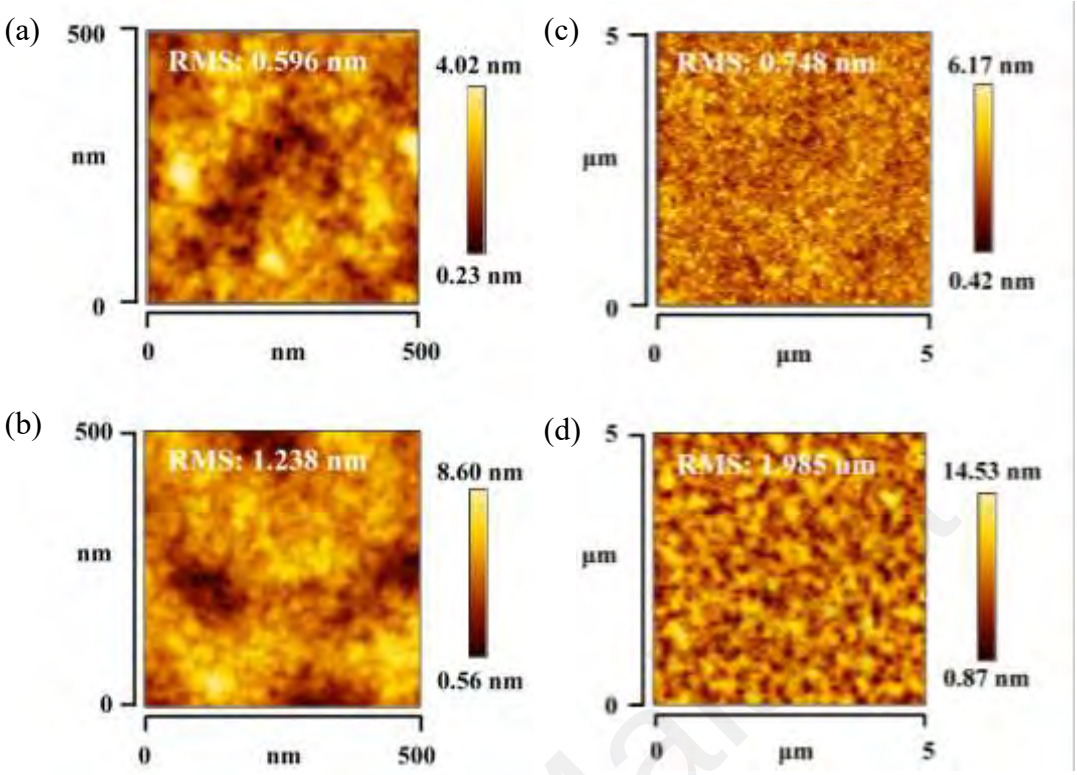

Figure 4.11: AFM images of P3HT:OXCBA thin film of ratio 1:0.50 with a scan size of (a) 0.5x0.5 µm and (b) 5x5 µm, while (c) and (d) for ratio 1:1.50 with a scan size of 0.5x0.5 µm and 5x5 µm, respectively.

The AFM images, seen in Figure 4.11(a)-(d) portrays the surface morphology of P3HT:OXCBA thin films with a scan size of 0.5 x 0.5 µm and 5 x 5 µm. From the AFM analysis, the surface root-mean-square (RMS) roughness for the composite film of 1:0.50 is obtained as 0.596 nm and 0.748 nm while the surface roughness of 1:1.50 thin film is found to be 1.238 nm and 1.985 nm, respectively. It can be seen that the P3HT:OXCBA thin film of 1:0.50 ratio exhibits a smoother surface than 1:1.50.

In general, a smoother surface indicates a well-mixed blend morphology and provide a better contact for the donor and acceptor interpenetrating network. According to Jonda et al, a homogeneous layer could reduce the possibility of short circuit and the formation of hot spots and dark spots (Jonda, Mayer, Stolz, Elschner, & Karbach, 2000). Even though the molecular weight of a material plays an important role in the crystallinity of the blend, the amount of OXCBA content is also found to be correlated with the

concentration of small molecule clusters in the blend. As small molecule fullerene derivatives retain much higher molecular mobility compared to polymers, optimizing the concentration of OXCBA can ensure the diffusion of OXCBA into the P3HT matrix, leading to the formation of an interpenetrating network, which at the same time enhancing the carrier transfer, and improving the overall device performance.

However, when the increase of concentration is out of the optimal composition, the small molecules are not homogeneously dispersed. They have the tendency to diffuse out of the polymer matrix and create a phase-separated cluster, thus affecting the blended morphology. This might also provide mechanical stress on the metal electrode, thereby possibly damaging the interface leading to poorer device performance. It can be inferred that mixing an appropriate amount of OXCBA may hinder the crystallization of P3HT in the blended film. Accordingly, it can be stated that the 1:0.50 blend ratio possesses molecular morphology which is more favourable for the transport of charge carriers and will provide better device performance.

4.3 Photodegradation Study of optimized P3HT:OXCBA OPD.

Figure 4.12 demonstrated that the EQE spectrum of the P3HT:OXCBA optimized device (ratio 1:0.50) is consistent with the absorption range of the blended film. It is expected that EQE increases from the dark states into high illumination absorption states and the EQE efficiency is larger when more photons are being generated and accumulated. The responsivity of the device is also assumed to increase with a larger EQE value (Hamilton & Kanicki, 2004). According to the graph, EQE increases steadily at a wavelength between 300 and 650 nm with a maximum of 52.77%. This proves that the combination of these materials with the optimized ratio of 1:0.50 exhibits great performance making it to be a suitable candidate in the application of a photodetector.

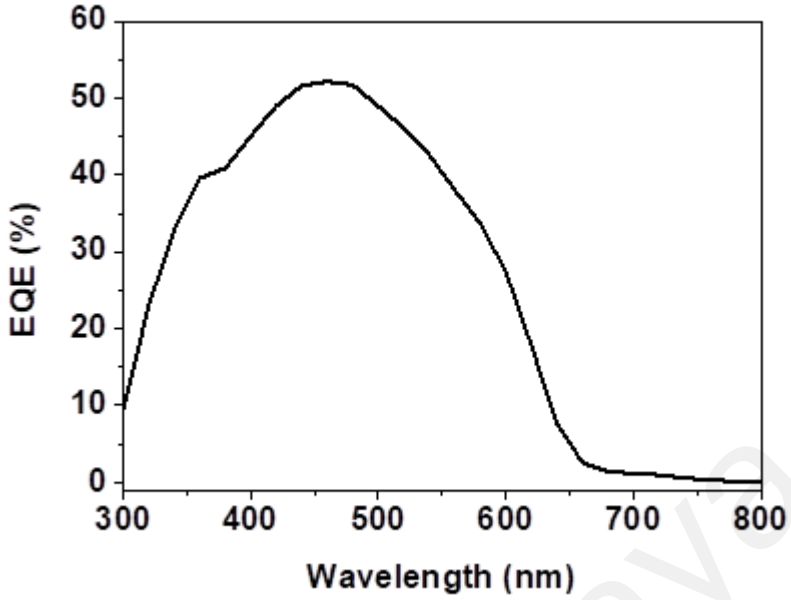

Figure 4.12: EQE spectrum of P3HT:OXCBA optimized device (1:0.50).

Despite having a good performance, device stability remains a crucial challenge in organic-based devices. To alleviate this issue, a stability test for the optimized device was carried out for 336 hours and a gradual reduction in its R from 252.69 mA/W to about 159.96 mA/W was found for over two-week time. The changes for this degradation trend are shown in Figure 4.13. The R and D* of the optimized device managed to retain at least 70% of its actual values even after 336 hours in the air atmosphere. As the device was encapsulated, the chance for oxygen and moisture uptake was rare, thus the degradation is attributed to light illumination as the device was exposed to light for a long time (Sherafatipour et al., 2019). The local motions of C-H and/or C-O-C atoms may also cause intrinsic photodegradation which affects the bonds rearrangement, resulting in midgap defect density and interface density along with an increment in the device resistance.

Besides, the active layer might exhibit macro-phase separation between the blend component when the device was illuminated for a long period of time. The cluster would

act as a trapping centre where carriers would accumulate and enhance trap-assisted recombination loss. The accumulated carrier could affect the electrostatic potential of the device, leading to the reduction in exciton diffusion length and exciton dissociation. It would also reduce the mobility upon absorption of photons, carrier transport and carrier collection efficiency.

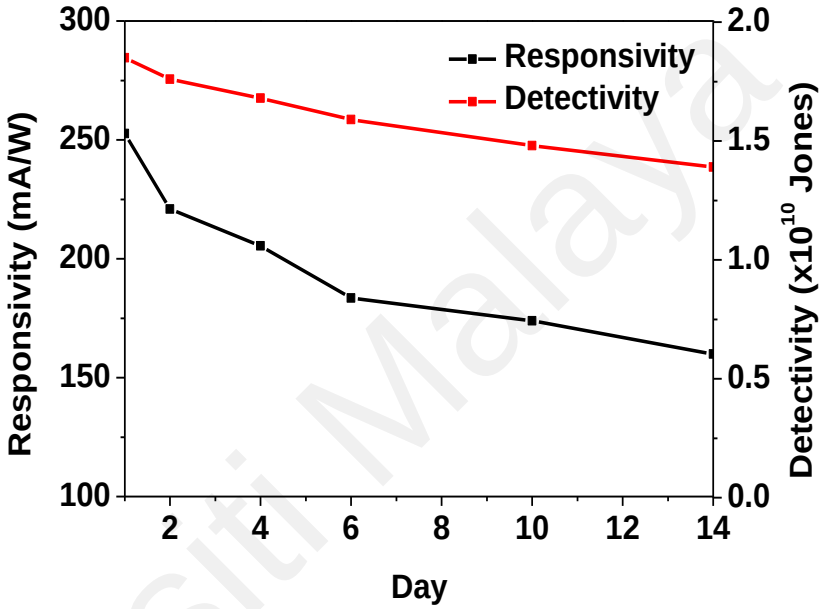

Figure 4.13: Stability behaviour of P3HT:OXCBA device with ratio 1:0.50 observed for 14 days.

CHAPTER 5: CONCLUSION AND FUTURE WORKS

5.1 Conclusion

The attempts to replace inorganic semiconductor with organic counterparts in many applications are tremendously increasing as green energy emerges as the next industry trends. A huge focus is being made to discover high potential material due to the importance of conserving energy for the growth of future generation. In this context, this thesis presents an in-depth study on the properties of OXCBA as a future competitor to PCBM and investigates its photosensing capability with P3HT. To achieve this goal, several techniques have been used to investigate the properties of thin film, especially OXCBA.

Firstly, the chemical properties of the material are observed using XPS. This gives us information on the chemical composition of the material. Next, the optical properties of the OXCBA and P3HT are measured using UV-Vis spectroscopy. OXCBA provides light absorption at a low optimal wavelength while P3HT covers intense absorption in the visible range. By blending both materials, a wider light absorption range is achieved as both materials cover different ranges of spectrum**.** Then, proper energy level alignment of P3HT and OXCBA are confirmed through UPS and detailed analysis on the electrical performance of the OPD is performed using I-V. The results from PL and AFM are also well matched with results observed from UV-Vis. In addition to that, Raman was also conducted to investigate the molecular vibration properties of OXCBA and P3HT:OXCBA blend. Lastly, the electrical performance of the optimized OPD of ratio 1:0.50 was performed by observing the EQE efficiency and its stability for over two weeks.

Various parameters such as responsivity and detectivity were considered and optimized to produce efficient OPD devices. The optimized device exhibits good

responsivity at 252.69 mA/W including acceptable rise and decay time of 445 ms and 309 ms, respectively. A high detectivity limit of 1.85 x 10^{10} Jones is obtained and its stability is retained at least 70% from its actual value. To sum up, we demonstrated that the insertion of OXCBA into a donor polymer matrix has a great potential in the light-sensing application and may contribute to the commercialization of high-performance photodetection application without any complicated fabrication.

5.2 Future work

There is still more work that needs to be done to prove that OPD is a promising alternative for the next generation photosensing application. Hence, we propose the following recommendation to be considered as potential future works. Although it is shown that organic material has many possibilities to be used for the photodetection applications, actual demonstration of large-area sensors integrated with organic photodetectors was not accomplished in this work. Therefore, we suggest developing a hybrid photosensor integrated with solution-processable organic photodetectors. Since the performance of the device reduces about 30% from its initial value after two weeks, this device may be integrated for disposal organic electronic application such as in health monitoring. This application has the advantage of short-term usage and allows the device to be used immediately before degraded.

REFERENCES

Abdullah, S. M., Rafique, S., Azmer, M. I., Jilani, A., Sajith, V. K., & Supangat, A. (2018). Modified photo-current response of an organic photodiode by using V2O5 in both hole and electron transport layers. *Sensors and Actuators A: Physical, 272*, 334-340.

Acevedo-Peña, P., Baray-Calderón, A., Hu, H., González, I., & Ugalde-Saldivar, V. M. J. J. o. S. S. E. (2017). Measurements of HOMO-LUMO levels of poly (3-hexylthiophene) thin films by a simple electrochemical method. *Journal of Solid State Electrochemistry, 21*(8), 2407-2414.

Adams, W. G., & Day, R. E. (1877). IX. The action of light on selenium. *Philosophical Transactions of the Royal Society of London, 167*, 313-349.

Ahmad, Z., Abdullah, S. M., & Sulaiman, K. (2013). Bulk heterojunction photodiode: To detect the whole visible spectrum. *Measurement, 46*, 2073–2076.

An, T., Wang, Y., & Xue, J. (2019). Optimization of the response spectra of organic photodetectors based on P3HT:PC61BM using PCPDTBT as the third component. *Optical and Quantum Electronics, 52*(1), Article#7.

Azimy, A., Hosseini, S., & Ramezanian, N. (2016). Investigation of Donor/acceptor Composition Ratio and Annealing Effects on Performances of Organic Solar Cells based on P3HT:C60. *Journal of Photopolymer Science and Technology, 29*, 775-780.

Ballantyne, A. M., Chen, L., Dane, J., Hammant, T., Braun, F. M., Heeney, M., . . . Nelson, J. (2008). The Effect of Poly(3-hexylthiophene) Molecular Weight on Charge Transport and the Performance of Polymer:Fullerene Solar Cells. *Advanced Functional Materials, 18*(16), 2373-2380.

Benten, H., Mori, D., Ohkita, H., & Ito, S. (2016). Recent research progress of polymer donor/polymer acceptor blend solar cells. *Journal of Materials Chemistry A, 4*(15), 5340-5365.

Bernardo, B., Cheyns, D., Verreet, B., Schaller, R. D., Rand, B. P., & Giebink, N. C. (2014). Delocalization and dielectric screening of charge transfer states in organic photovoltaic cells. *Nature Communications, 5*(1), Article#3245.

Brebels, J., Manca, J. V., Lutsen, L., Vanderzande, D., & Maes, W. (2017). High dielectric constant conjugated materials for organic photovoltaics. *Journal of Materials Chemistry A, 5*(46), 24037-24050.

Costa, J. C. S., Taveira, R. J. S., Lima, C. F. R. A. C., Mendes, A., & Santos, L. M. N. B. F. (2016). Optical band gaps of organic semiconductor materials. *Optical Materials, 58*, 51-60.

Dang, M. T., Hirsch, L., & Wantz, G. (2011). P3HT:PCBM, Best Seller in Polymer Photovoltaic Research. *Advanced Materials, 23*(31), 3597-3602.

Dechun, Z. (2013). 4 - Chemical and photophysical properties of materials for OLEDs. In A. Buckley (Ed.), *Organic Light-Emitting Diodes (OLEDs)* (pp. 114-142): Woodhead Publishing.

Eastham, N. D., Dudnik, A. S., Harutyunyan, B., Aldrich, T. J., Leonardi, M. J., Manley, E. F., . . . Marks, T. J. (2017). Enhanced Light Absorption in Fluorinated Ternary Small-Molecule Photovoltaics. *ACS Energy Letters, 2*(7), 1690-1697.

Greczynski, G., & Hultman, L. (2020). X-ray photoelectron spectroscopy: Towards reliable binding energy referencing. *Progress in Materials Science, 107*, Article#100591.

Guan, Z.-L., Bok Kim, J., Loo, Y.-L., & Kahn, A. J. J. o. A. P. (2011). Electronic structure of the poly (3-hexylthiophene): indene-C60 bisadduct bulk heterojunction. *Journal of Applied Physics, 110*(4), Article#043719.

Hamilton, M. C., & Kanicki, J. (2004). Organic polymer thin-film transistor photosensors. *IEEE Journal of Selected Topics in Quantum Electronics, 10*(4), 840-848.

Han, Y., Zhang, X., Zhang, F., Zhao, D., & Yu, J. (2019). Improved charge transfer, mobility and morphology for high performance panchromatic organic photodetectors by adding PC71BM in P3HT:IEICO-4F. *Organic Electronics, 75*, Article#105410.

Helander, M. G., Greiner, M. T., Wang, Z. B., & Lu, Z. H. (2010). Pitfalls in measuring work function using photoelectron spectroscopy. *Applied Surface Science, 256*(8), 2602-2605.

Holliday, S., Ashraf, R. S., Wadsworth, A., Baran, D., Yousaf, S. A., Nielsen, C. B., . . . McCulloch, I. (2016). High-efficiency and air-stable P3HT-based polymer solar cells with a new non-fullerene acceptor. *Nature Communications, 7*(1), Article#11585.

Itskos, G., Othonos, A., Rauch, T., Tedde, S. F., Hayden, O., Kovalenko, M. V., . . . Choulis, S. A. (2011). Optical Properties of Organic Semiconductor Blends with Near-Infrared Quantum-Dot Sensitizers for Light Harvesting Applications. *Advanced Energy Materials, 1*(5), 802-812.

Ji, C. H., Lee, S. J., & Oh, S. Y. (2019). P3HT-based visible-light organic photodetectors using PEI/PAA multilayers as a p-type buffer layer. *RSC Advances, 9*(64), 37180-37187.

Jonda, C., Mayer, A. B. R., Stolz, U., Elschner, A., & Karbach, A. (2000). Surface roughness effects and their influence on the degradation of organic light emitting devices. *Journal of Materials Science, 35*(22), 5645-5651.

Kadem, B., Hassan, A., & Cranton, W. (2016). Efficient P3HT:PCBM bulk heterojunction organic solar cells; effect of post deposition thermal treatment. *Journal of Materials Science: Materials in Electronics, 27*(7), 7038-7048.

Kallmann, H., & Pope, M. (1959). Photovoltaic Effect in Organic Crystals. *The Journal of Chemical Physics, 30*(2), 585-586.

Kang, D. J., Kang, H., Cho, C., Kim, K.-H., Jeong, S., Lee, J.-Y., & Kim, B. J. J. N. (2013). Efficient light trapping in inverted polymer solar cells by a randomly nanostructured electrode using monodispersed polymer nanoparticles. *Nanoscale, 5*(5), 1858-1863.

Kang, H., Kim, K.-H., Kang, T. E., Cho, C.-H., Park, S., Yoon, S. C., & Kim, B. J. (2013). Effect of Fullerene Tris-adducts on the Photovoltaic Performance of P3HT:Fullerene Ternary Blends. *ACS Applied Materials & Interfaces, 5*(10), 4401-4408.

Kielar, M., Dhez, O., Pecastaings, G., Curutchet, A., & Hirsch, L. (2016). Long-Term Stable Organic Photodetectors with Ultra Low Dark Currents for High Detectivity Applications. *Scientific Reports, 6*(1), Article#39201.

Kim, G.-H., Kim, H.-B., Walker, B., Choi, H., Yang, C., Park, J., & Kim, J. Y. (2013). Effects of Ionic Liquid Molecules in Hybrid PbS Quantum Dot–Organic Solar Cells. *ACS Applied Materials & Interfaces, 5*(5), 1757-1760.

Kim, H., Park, J., Grimsdale, A., & Hwang, D.-H. (2015). Methyl and Dimethyl o-Xylenyl-Substituted Fullerene Acceptors for Polymer Solar Cells. *Israel Journal of Chemistry, 55*: 1017-1027.

Kim, H., Park, O., Park, J., & Hwang, D.-H. (2016). Trimethylsilyl o-Xylenyl-Substituted Fullerene Bis-Adduct as Electron Acceptor for Solution-Processed Polymer Solar Cells. *Journal of Nanoscience and Nanotechnology, 16*, 10465-10469.

Kim, H. J., Kim, J.-H., Ryu, J.-H., Kim, Y., Kang, H., Lee, W. B., . . . Kim, B. J. (2014). Architectural Engineering of Rod–Coil Compatibilizers for Producing Mechanically and Thermally Stable Polymer Solar Cells. *ACS Nano, 8*(10), 10461-10470.

Kim, K.-H., Kang, H., Kim, H. J., Kim, P. S., Yoon, S. C., & Kim, B. J. (2012). Effects of Solubilizing Group Modification in Fullerene Bis-Adducts on Normal and Inverted Type Polymer Solar Cells. *Chemistry of Materials, 24*(12), 2373-2381.

Kim, K.-H., Kang, H., Nam, S. Y., Jung, J., Kim, P. S., Cho, C.-H., . . . Kim, B. J. (2011). Facile Synthesis of o-Xylenyl Fullerene Multiadducts for High Open Circuit Voltage and Efficient Polymer Solar Cells. *Chemistry of Materials, 23*(22), 5090-5095.

Lee, C.-C., Biring, S., Ren, S.-J., Li, Y.-Z., Li, M.-Z., Al Amin, N. R., & Liu, S.-W. (2019). Reduction of dark current density in organic ultraviolet photodetector by utilizing an electron blocking layer of TAPC doped with MoO3. *Organic Electronics, 65*, 150-155.

Lee, T. H., Park, S. Y., Du, X., Park, S., Zhang, K., Li, N., . . . Kim, J. Y. (2020). Effects on Photovoltaic Characteristics by Organic Bilayer- and Bulk-Heterojunctions: Energy Losses, Carrier Recombination and Generation. *ACS Applied Materials & Interfaces, 12*(50), 55945-55953.

Li, W., & Kwok, H. (2012). Conduction Mechanisms in Organic Semiconductors. In B. Bhushan (Ed.), *Encyclopedia of Nanotechnology* (pp. 493-500). Dordrecht: Springer Netherlands.

Li, Y., Yu, L., Peng, C., Mao, L., Li, X., & Zhang, J. (2020). Top-Illuminated Flexible Organic Photodetectors Integrated With Hole Extraction Layers Synthesized With Solution-Processed NiO_x Films at Room Temperature. *IEEE Transactions on Electron Devices, 67*(10), 4308-4312.

Liu, X., Lin, Y., Liao, Y., Wu, J., & Zheng, Y. (2018). Recent advances in organic near-infrared photodiodes. *Journal of Materials Chemistry C, 6*(14), 3499-3513.

Maeng, M., Kim, J.-H., Hong, J.-A., & Park, Y. (2016). Effects of oxygen plasma treatments on the work function of indium tin oxide studied by in-situ photoelectron spectroscopy. *Journal of the Korean Physical Society, 68*, 692-696.

Mayerhöfer, T. G., Mutschke, H., & Popp, J. (2016). Employing Theories Far beyond Their Limits—The Case of the (Boguer-) Beer–Lambert Law. *ChemPhysChem: a European Journal of Chemical Physics and Physical Chemistry, 17*(13), 1948-1955.

Moliton, A., & Hiorns, R. C. (2012). The origin and development of (plastic) organic electronics. *Polymer International, 61*(3), 337-341.

Niu, C., Zhu, T., & Lv, Y. (2019). Influence of Surface Morphology on Absorptivity of Light-Absorbing Materials. *International Journal of Photoenergy, 2019*, Article#1476217.

Pei, Z., Devi, B., & Subramani, T. (2014). Study on the Al–P3HT:PCBM interfaces in electrical stressed polymer solar cell by X-ray photoelectron spectroscopy. *Solar Energy Materials and Solar Cells, 123*, 1–6.

Salamandra, L., La Notte, L., Fazolo, C., Di Natali, M., Penna, S., Mattiello, L., . . . Reale, A. (2020). A comparative study of organic photodetectors based on P3HT and PTB7 polymers for visible light communication. *Organic Electronics, 81*, Article#105666.

Sariciftci, N. S., Smilowitz, L., Heeger, A. J., & Wudl, F. A. (1992). Photoinduced Electron Transfer from a Conducting Polymer to Buckminsterfullerene. *Science (New York, N.Y.), 258*, 1474-1476.

Shafian, S., Jang, Y., & Kim, K. (2015). Solution processed organic photodetector utilizing an interdiffused polymer/fullerene bilayer. *Optics Express, 23*(15), A936-946.

Sherafatipour, G., Benduhn, J., Patil, B. R., Ahmadpour, M., Spoltore, D., Rubahn, H.-G., . . . Madsen, M. (2019). Degradation pathways in standard and inverted DBP-C70 based organic solar cells. *Scientific Reports, 9*(1), Article#4024.

Shirakawa, H., Louis, E. J., MacDiarmid, A. G., Chiang, C. K., & Heeger, A. J. (1977). Synthesis of electrically conducting organic polymers: halogen derivatives of

polyacetylene, (CH). *Journal of the Chemical Society, Chemical Communications*(16), 578-580.

Shirakawa, H., McDiarmid, A., & Heeger, A. (2003). Focus Article: Twenty-Five Years of Conducting Polymers. *Chemical Communications, 2*, 1-4.

Singh, A., Dey, A., & Iyer, P. K. (2017). Influence of molar mass ratio, annealing temperature and cathode buffer layer on power conversion efficiency of P3HT:PC71BM based organic bulk heterojunction solar cell. *Organic Electronics, 51*, 428-434.

Singh, S. P., Sellinger, A., & Dodabalapur, A. (2010). Electron transport in copper phthalocyanines. *Journal of Applied Physics, 107*(4), Article#044509.

Tajbakhsh, M., Kariminasab, M., Ganji, M. D., & Alinezhad, H. (2017). Molecular design of novel fullerene-based acceptors for enhancing the open circuit voltage in polymer solar cells. *Journal of Physics and Chemistry of Solids, 111*, 410-418.

Tang, C. W. (1986). Two-layer organic photovoltaic cell. *Applied Physics Letters, 48*(2), 183-185.

Treat, N. D., Brady, M. A., Smith, G., Toney, M. F., Kramer, E. J., Hawker, C. J., & Chabinyc, M. L. (2011). Interdiffusion of PCBM and P3HT Reveals Miscibility in a Photovoltaically Active Blend. *Advanced Energy Materials, 1*(1), 82-89.

Tremel, K., & Ludwigs, S. (2014). Morphology of P3HT in thin films in relation to optical and electrical properties. In *P3HT Revisited–From Molecular Scale to Solar Cell Devices* (pp. 39-82): Springer.

Wei, H., Scudiero, L., & Eilers, H. (2009). Infrared and photoelectron spectroscopy study of vapor phase deposited poly (3-hexylthiophene). *Applied Surface Science, 255*(20), 8593-8597.

Xiao, b., Tang, A., Yang, J., Wei, Z., & Zhou, E. (2017). P3HT-Based Photovoltaic Cells with a High V oc of 1.22 V by Using a Benzotriazole-Containing Nonfullerene Acceptor End-Capped with Thiazolidine-2,4-dione. *ACS Macro Letters, 6*, 410-414.

Xu, X., Zhang, G., Yu, L., Li, R., & Peng, Q. (2019). P3HT-Based Polymer Solar Cells with 8.25% Efficiency Enabled by a Matched Molecular Acceptor and Smart Green-Solvent Processing Technology. *Advanced Materials, 31*(52), Article#1906045.

Xu, Y., Wang, X., Zhou, J., Song, B., Jiang, Z., Lee, E., . . . Chen, G. (2018). Molecular engineered conjugated polymer with high thermal conductivity. *Science Advances, 4*(3)*, eaar3031*.

Yang, D., & Ma, D. (2019). Development of Organic Semiconductor Photodetectors: From Mechanism to Applications. *7*(1), Article#1800522.

Yu, G., & Heeger, A. J. (1995). Charge separation and photovoltaic conversion in polymer composites with internal donor/acceptor heterojunctions. *Journal of Applied Physics, 78*(7), 4510-4515.

Zhang, G., Zhang, K., Yin, Q., Jiang, X.-F., Wang, Z., Xin, J., . . . Cao, Y. (2017). High-Performance Ternary Organic Solar Cell Enabled by a Thick Active Layer Containing a Liquid Crystalline Small Molecule Donor. *Journal of the American Chemical Society, 139*(6), 2387-2395.

Zhao, Z., Xu, C., Niu, L., Zhang, X., & Zhang, F. (2020). Recent Progress on Broadband Organic Photodetectors and their Applications. *Laser & Photonics Reviews*, 14, Article#2000262.

Zhokhavets, U., Erb, T., Gobsch, G., Al-Ibrahim, M., & Ambacher, O. (2006). Relation between absorption and crystallinity of poly(3-hexylthiophene)/fullerene films for plastic solar cells. *Chemical Physics Letters, 418*(4), 347-350.

Zworykin, V. K., Morton, G. A., & Malter, L. (1936). The Secondary Emission Multiplier-A New Electronic Device. *Proceedings of the Institute of Radio Engineers, 24*(3), 351-375.